NTNU
Norwegian University of
Science and Technology

Shaly Sand Formation Evaluation from logs of the Skrugard well, Southwestern Barents Sea, Norway

Marco Shaban Lutome

Petroleum Geosciences
Submission date: July 2016
Supervisor: Erik Skogen, IPT

Norwegian University of Science and Technology
Department of Petroleum Engineering and Applied Geophysics

Norwegian University of Science and Technology

Department of Petroleum Engineering and Applied Geophysics

MSC THESIS IN PETROLEUM GEOSCIENCE

Shaly Sand Formation Evaluation from logs of the Skrugard well, Southwestern Barents Sea, Norway

By

Marco Shaban Lutome

Supervisor: Erik Skogen

Acknowledgement

I would like to express my special thanks to: STATOIL for providing financial support during the entire period of my study in Norway and in Tanzania; the Norwegian University of Science and Technology (NTNU) for providing good environment for my study; the University of Dar Es Salaam for running and coordinating the program; Erik Skogen for your supervision and instruction you made during Thesis writing as it would be hard without your direction you made; and my fellow ATHEI students for the encouragement and contribution you shown.

I would like to thank my family for motivation, encouragement, and support you shown during my study time.

Abstract

Archie`s interpretation model to estimate water saturation in clean formations has successfully been useful over the years. However, in shaly sand formation this model yields inaccurate water saturation estimates (overestimate) due to shale or clay effects. Many shaly sand interpretation models have been developed; unfortunately; there is no unique model that appears to fit all shaly sand reservoirs.

A comparison study of water saturation on well 7220/8-1 was carried out using four different saturation models (Archie, Indonesian, Simandoux, and Modified Simandoux). Formation permeability was then estimated using two NMR permeability models (Timur-Coates and SDR).

The results from the study have shown that the average water saturation values from Archie model (14.3%) were higher than that of shaly models. The Indonesian model yields average water saturation value of 13.6% which is close to that given by Archie model. The result from the Simandoux model is 12.8% which is slightly lower than that of Archie model but close to Indonesian model. The even lowest average water saturation (9.8%) is obtained from the Modified Simandoux model. The average permeability values were 1837 mD and 566 mD for Timur-Coates and SDR models respectively.

The Modified Simandoux model is the most optimistic for the study due to its lowest average water saturation value. The NMR Timur-Coates permeability is again the most optimistic model due to its relatively good agreement with the core-derived permeability.

Table of Contents

List of Figures

List of Tables

Nomenclature

a = tortuosity of the rock, unit less

BVI = Bound fluid volume (%)

BVM = Free fluid volume (%)

C = permeability constant (unitless)

CEC = Cation exchange capacity (meq/mg)

C_PERM = Core permeability (mD)

C_POR = Core porosity (frac)

C_{sh} = shale conductivity (mho/m)

C_t = total formation conductivity (mho/m)

C_w = conductivity of formation water (mho/m)

DMRP = Density Magnetic Resonance Porosity, (v/v).

DPHI = Density porosity (v/v)

GOC = Gas oil contact

GR = Gamma ray, API.

I_{GR} = Gamma ray index.

K = Permeability (mD)

OWC = Oil water contact

m = Cementation exponent, dimensionless

n = Saturation exponent, dimensionless

N-D = Neutron-Density porosity logs.

PHE = Effective porosity from neutron-density logs (v/v).

ø = Formation porosity, (v/v).

R_{sh} = Shale formation resistivity, Ohoms-meter.

R_t = Formation resistivity, ohms-meter

R_w = Formation water resistivity, ohms-meter.

SW_AR = Archie water saturation, (v/v).

S_{wavg} = Average water saturation

SWE_INDO = Effective Indonesian water saturation, (v/v).

SWE_SIM = Effective Simandoux water saturation, (v/v).

S_w = Water saturation

TCMR = Total combinable magnetic resonance (v/v)

T_{2GM} = Geometric mean of NMR distribution (ms)

V_{sh_GR} = Volume of shale calculated from gamma ray log, (v/v).

V_{sh_ND} = Volume of shale from neutron-density porosity logs, (v/v)

1 INTRODUCTION

Shales are generally conductive that complicates petrophysical interpretation and evaluation and therefore mask or obscure the high resistance characteristics of hydrocarbons (Darling 2005). The nature and properties of shales or clays affects various log responses in different ways by under-or overestimating the measured values. The use of Archie equation to estimate water saturation, (S_w) in clean hydrocarbon bearing reservoir has successfully been useful over many years. However, in shaly formation this approach misleads the results by overestimating the water saturation value due to extra conductivity contribution from clays or shales.

To alleviate the problem of overestimating water saturation by Archie many shaly-sand interpretation models have been developed that accommodate the extra conductivity of shales (C_{sh}). Unfortunately, there is no specific model that predominates over the other within petroleum industry due to varying shale contents and distributions. Furthermore, the application of these models is influenced by many factors such as water resistivity (R_w). For instance Indonesian and Simandoux model demands high and low R_w values respectively. The purpose of the study is to apply and compare the shaly-sand interpretation models` results to the basic Archie`s results for the reservoir found in the Stø and Nordmela Formations in the Barents Sea. Shaly-sand saturation models yields S_w values that are less than that given by Archie`s model**.** How much water saturation values of shaly-sand models differs from that of Archie`s model**.** Due to unavailability of core and production test results any method that tends to give similar or close value to Archie`s value can be considered to be pessimistic.

The selected shaly-sand interpretation models include Indonesian, Simandoux, and modified Simandoux. However, if core data is available other shaly-sand based core data evaluation models can be used such as Waxman-Smits. These models produce more accurate results because their model parameters and shale properties are derived from core analysis.

1.1 Project Outline

To accomplish the objectives, the project will be carried out using Schlumberger`s Software (Techlog). Data sorting or data quality control is performed at the early stage before qualitative and quantitative interpretation is performed.

The study is organized in the following ways: Introduction part- description of the study area and background of clay minerals, Literature review- describes the theory of the presented topic, Methodology-describes in details the evaluation steps as performed in Techlog, Qualitative interpretation-provides detailed information of the lithology and possible contained fluids from well logs, Results and discussion-presentation of figures, tables, and arguments of the findings, and lastly is the Conclusion and recommendations which gives specific judgments of the arguments and possible suggestions of the lack or gap that have to be improve.

1.2 Objective.

1.2.1 Main Objective

The main objective of the study is to perform petrophysical evaluation both qualitative and quantitative of the Johan Castberg discovery well (7220/8-1).

1.2.2 Specific Objectives

The Thesis is derived by the following specific objectives.

I. Lithology and fluid interpretation from well log characteristics (signature) and neutron-density crossplot.
II. Determination of shale distribution using Thomas-Stieber technique.
III. Porosity, water saturation, and permeability determination
IV. Determination of hydrocarbon moveability index.

1.3 Study Area

The well 7220/8-1 was drilled west of the Polheim Sub-platform and Loppa High in the Barents Sea in 2011 and proved oil and gas (later named ´Johan Castberg´). It is located about 110 kilometres north of the Snøhvit field, west of the Loppa High with the water depth of about 370 metres. Above the reservoir the well penetrated Tertiary and Cretaceous Claystones and Sandstone and upper Jurassic Claystones. Further down in the reservoir it penetrated Sandstones of Jurassic age within Stø, Nordmela, and Tubåen formations as well as within Fruholmen and Snadd Formations where it penetrated Sandstones of Triassic age. **Figure 1** illustrates the stratigraphic column of these Formations.

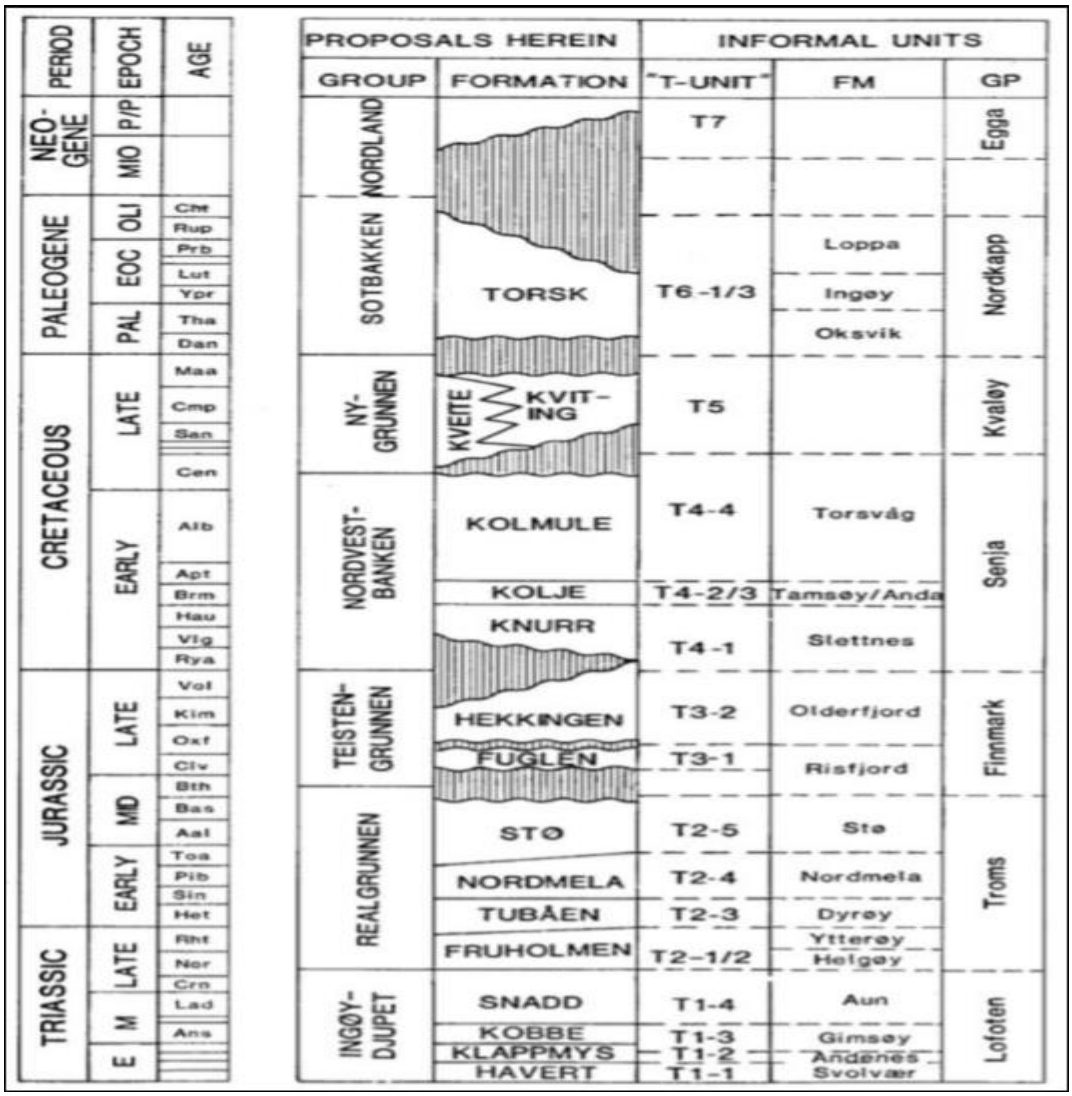

Figure 1: A lithostratigraphic scheme for the Mesozoic and Cenozoic succession offshore Norway (Dalland et al., 1988)

The well penetrated reservoir with top Stø and Nordmela Formations at the depth of about 1276m and 1354m respectively. Stø and Nordmela Formations contain a 37m thick gas column to 1312m (GOC) and 83m thick oil column to 1395m (OWC). In fact, oil and gas were discovered in the Stø and Nordmela Formation where there was a good showing of hydrocarbons during drilling from cuttings and core chips and nothing beyond 1400m within the well (NPD). Location of the study area is shown in **Figure 2**.

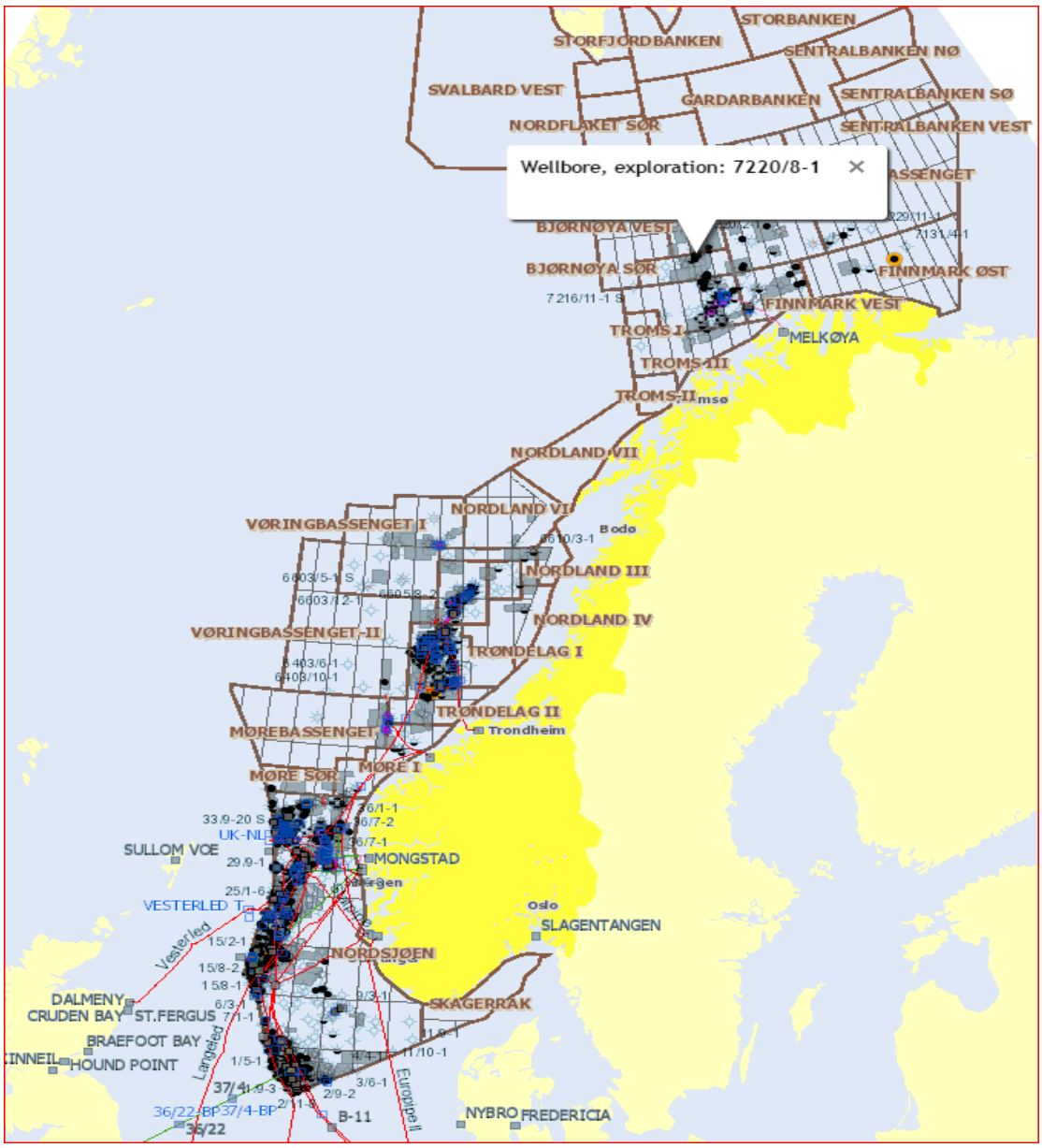

Figure 2: Map of the study area showing well location (Source: NPD)

1.4 Geological Setting and Stratigraphy of the Barents Sea.

Geologically, the Barents Sea is a complex of basins and platforms bracketed by the north Norwegian and Russian coasts, and the eastern margin of the deep Atlantic Ocean. The area of the Barents Sea is about 1.3 million Km^2 with water depth averaging to about 300m. It was originally formed by two major continental collisions and subsequently followed by continental separation (Doré 1995). The uplift of the Barents Sea is related to thermal effect due to north Atlantic rifting accompanied with an opening, isotactic adjustments caused by glaciation and erosion is the another source of uplift of the Barents Sea (Riis and Fjeldskaar 1992).

The stratigraphy of the Barents Sea mainly comprises of carbonates and clastic sediments. Until the Late Permian limestone and dolostones dominated with thick salt deposit in the Nordkapp Basin. The Upper Permian through the Triassic the Barents Sea is dominated by marine and alluvial shales and some sandstone layers reflecting numerous transgressive and regressive episodes of the Triassic. The Uppermost Triassic to Middle Jurassic is sandier indicating high-energy depositional environment. From the Upper Jurassic and Cretaceous is dominated by marine shale suggesting a more distal environment. As a consequence of uplift and erosion, the Late Cretaceous and Tertiary sediments have been partially remove (Ohm, Karlsen et al. 2008).

Most of reservoirs in the Barents Sea are the Early Jurassic sandstones deposited in a coastal-plain Nordmela Formation and shallow marine Stø Formation. The reservoir rocks were overlain by the organic-poor shales of the Fuglen Formation, which separates the Jurassic reservoirs from the Late Jurassic Hekkingen Formation. These rocks are presently overlain by cap rock shales of Cretaceous –Eocene age with thin limestone and dolomite layers in the Hammerfest Basin (Hermanrud, Halkjelsvik et al. 2014). The succession of the Formations is illustrated in **Figure 1** above.

1.5 Clays and Shale

The accurate estimation of hydrocarbon resources in shaly clastic reservoirs requires knowledge of clay minerals and shale. Clays are described in terms of rock and particles, as a rock, they earthy, fine-grained materials that undergo plasticity when mixed with small amount of water; as particles, they are less than 4μm in size (Ruhovets and Fertl 1982). Clay minerals are defined as hydrated silicates with a layer of chain lattices consisting of sheets of silica and tetrahedral arranged in hexagonal form alternating with octahedral layers and are usually of small size (Mackenzie 1959).

Most of the clay minerals have some substitution of aluminum by other cations, such as magnesium, iron, etc. The substitution process creates charge deficiency on the surface of clay minerals, making a room for cations from brine solution to be absorbed onto clay`s surface. CEC values of clay relate directly to their capacity to absorb and hold water. The montmorillonite (smectite) has the highest CEC and therefore have the highest capacity to absorb water. Kaolinite and chlorite on the other hand, have the lowest Cation Exchange Capacity (CEC) and low capacity to hold water on their surface. The portion of the water contained in the pores of shaly formations is closely associated with the clay mineral as hydration or bound water (Hill, Klein et al. 1979).

Shale can be defined as an earthy, fine-grained sedimentary rock with specific laminated character deposited in low energy environment. Shaly sand and shales have similar mineralogy because they are derived from the same source, transported and emptied into the basin by the same agent (river). Sand and shales are differentiated as the particles begin to settle at differing rates due to their particle size and transporting energy and not mineral type (Thomas and Stieber 1975).

Shaly sands behave as perm-selective cation-exchange membranes with their electrochemical efficiencies increases with increasing clay contents (Waxman and Smits 1968). The electrochemical behavior is related to the cation exchange capacity per unit pore volume of the rock (Hill, Klein et al. 1979). Montmorillonite has the highest cation exchange capacity due to its large

interlayer surfaces between sheet structures. Also, there is a close linear relationship between cation exchange capacity and specific surface area of the clay minerals (Ellis and Singer 2007). **Figure 3** Show the type and their associated properties.

Mineral	Specific surface area (m^2/g)	CEC (meq/100g)
Smectite	700–800	80–150
Illite	113	10–40
Chlorite	42	10–40
Kaolinite	15–40	3–5

Figure 3: typical values of Specific area, Cation Exchange Capacity and other properties of clay minerals (Ellis and Singer 2007)

1.6 Clay Types

Shaly clastic reservoir rocks often contain varying amount of different clays, each inhibits significant differences in their basic properties such as Cation Exchange Capacity (CEC), hydrogen index (HI), matrix density, chemical properties and composition (Fertl and Chilingar 1988). The clay mineral suite mainly consists of kaolinite, montmorillonite (smectite), illite, and chlorite. Clay minerals are aluminosilicate with a sheet-like structure containing aluminum and silicon atoms. Each sheet consist octahedral sheet of oxygen or hydroxyl around a central atom (aluminum) sometimes iron or magnesium. The other sheet is tetrahedral units consists of central silicon atom surrounded by oxygen (Ellis and Singer 2007).

All the four types of clay minerals above are formed by different stacking combination of two sheet structures with a characteristics dimension or spacing as shown in **Figure 4**. Kaolinite, for example, has the simplest structures formed

by stacking of one octahedral sheet and tetrahedral sheet to form one layer and it is 1:1. The other groups are formed by stacking of two tetrahedral sheets sharing oxygen atoms with an octahedral sheet between them and it is 2:1.

In subsurface water is adsorbed on the surface of clays and is referred as clay bound water. Some of the clays such as smectite have water between the molecule sheets and this water is known to be interlayer water (La Vigne, Herron et al. 1994). The associated clay bound water is the primary source of lowering the formation resistivity observed during measurements because of additional conductivity contribution to formation conductivity from clays.

Clay minerals consist of hydroxyl group (OH^-) making hydrogen an integral part of their molecule structure. This is the source of separation between neutron and density in shale during logging and is used in interpretation for shale volume.

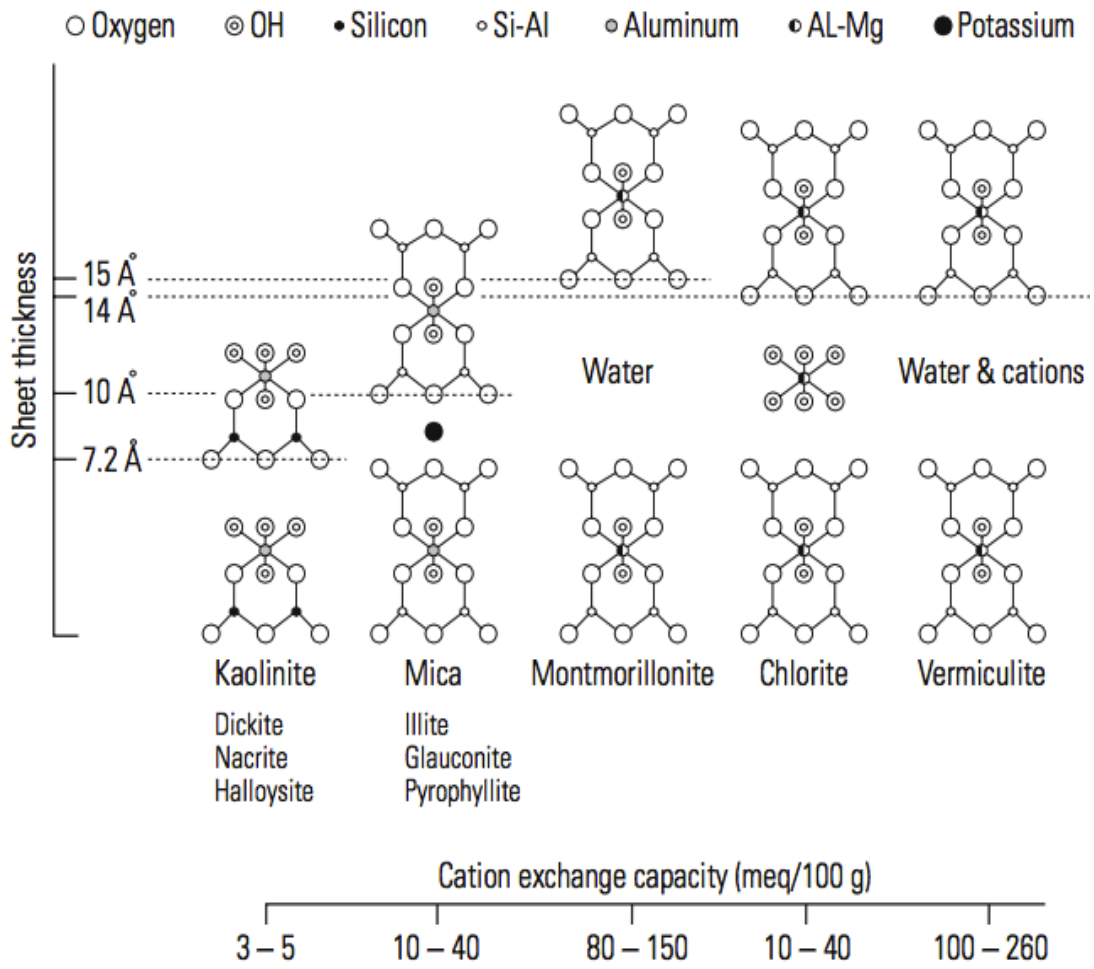

Figure 4: Systematic representation of the structure and composition of members of the five clay mineral groups (Ellis and Singer 2007)

1.7 Mode of shale distribution

Clay minerals in sandstone can have two distinct origins. Those formed at some point outside of sandstone framework (detrital origin) and incorporated into the sandstone shortly after deposition of sediments or may form locally within the sandstone framework (diagenetic origin) and this occurs as the products of recrystallization of the early formed minerals (Almon 1979).

Mainly, three modes of shale distribution have been distinguished in sandstone reservoirs, which are:

Laminated shale

Laminated shale occurs as thin beds or streaks of shale between layers of reservoir rocks **Figure 5** illustrates. This type of shale distribution does not

affect the effective porosity, saturation, and or permeability of intermediate permeable layer. Laminated shale is a vertical permeability barrier of the intermediate permeable beds. Laminated shales are considered to have the same properties as the adjacent thick shale beds because they are subjected to the same deposition conditions (compaction). The conductive system of laminar shales is in parallel with the more or less conductive beds. (Hamada and Al-Awad 2000).

Dispersed shales

Shale of this type occurs as the matrix within interstices grains by either coating the grains or completely filling the pore spaces between the grains **Figure 5**. Shaly sand formations possess different properties from the laminated shales since they are subjected to different conditions and constraints (Hamada and Al-Awad 2000). This type of dispersed shale in pore reduces the original porosity and permeability without affecting the original grain. (Ellis and Singer 2007).

The permeability of dispersed shaly sand formation is reduced following the available spaces for the fluid flow being restricted; the other effect is wettability effect of clay being higher than quartz. The effect is the increase in water saturation and a decrease in fluid mobility. The electrical conductivity of dispersed shale is a combination of pore fluids and dispersed clay and act as an assembly of conductors.

Structural shale

This category of shale forms as part of rock grains along with quartz and other grains. They have some common characteristics with laminated shale since they are deposited from the same diagnostic conditions. The effects of structural shale on permeability and resistivity resembles more similar to those of dispersed shales.

Generally, laminated shale is of deposition in original while the dispersed clays evolve from alteration of unstable minerals.

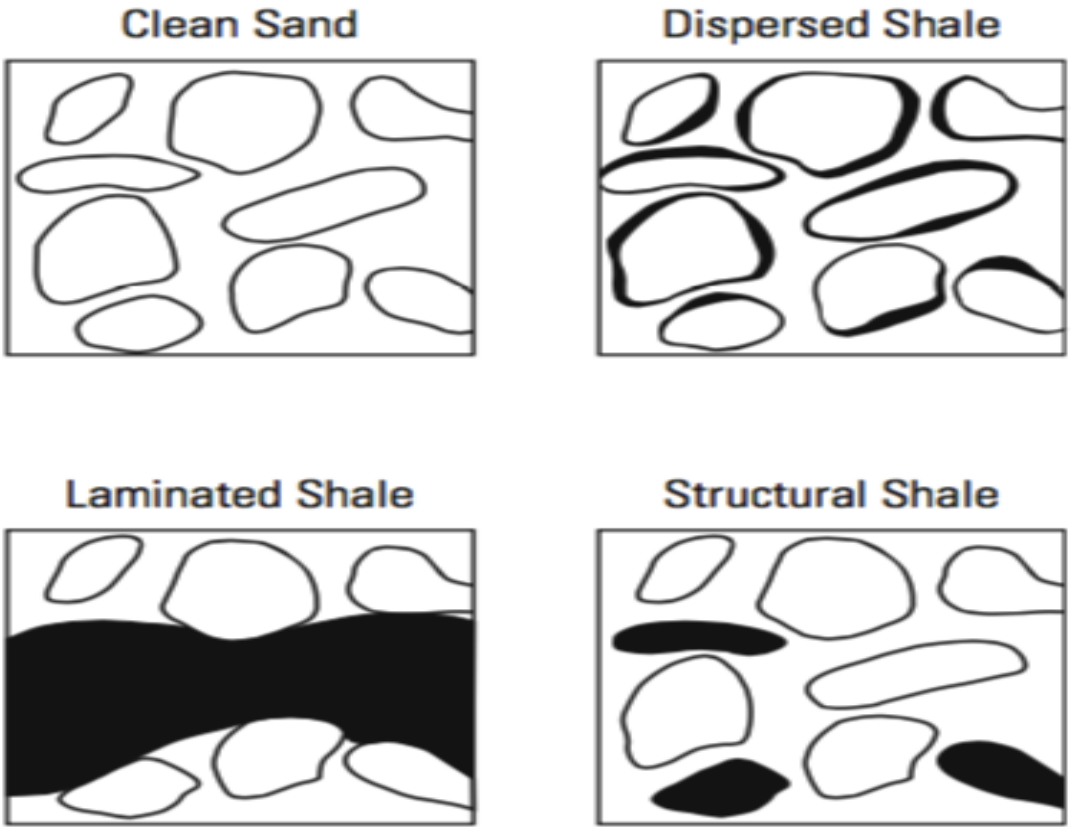

Figure 5: Shale distribution in sandstone (Ellis and Singer 2007)

1.8 Effects of Shaliness on Log response

Shaly-sand reservoirs often contain clay minerals, which introduces another conductive path for cations in the brine (De Waal 1989). Clay minerals have electrical charge deficiency that can be compensated (by positive or counter ions) to maintain electrical charge neutrality of the clay structure. The amount of these compensating ions constitutes to the so-called Cation Exchange Capacity (CEC) which is related to the surface area of the clay minerals (**Figure 3**). The positive ions provide an additional conductivity of the rock as they leave the surface of the clay.

There are two components associated with shaly formations; conductivity associated with free fluids filling porosity and that associated with Cation Exchange Capacity (CEC). The low resistivity anomaly caused by clay compensating ion can be regarded as a surface effect associated with clay grain and bound water associated with clay minerals (Hamada and Al-Awad 2000). It is therefore that, the low formation resistivity can also be associated with the

matrix instead of the clay bound water (Berg 1996). The conductivity of shaly sand depends on the shale type, the amount of shale and the way it distributed in the reservoir.

Clays in formation often affects porosity logs (density, neutron, sonic, etc) and hence complicates the determination of resistivity, porosity and saturation due to their associated properties, nature, and their distribution.

2 LITERATURE REVIEW

Shaly sand formation evaluation involves a number of steps; these include lithology and fluid identification, shale volume estimate, porosity estimates, water saturation estimates, and permeability estimates. This chapter outlines the concepts related to these parameters as used in the study.

2.1 Petrophysical Properties

Determination of petrophysical parameters is a paramount step in formation evaluation to determine the economic viability of hydrocarbon-bearing reservoirs (Fens, 2000).

2.1.1 Shale Volume (V_{sh})

The determination of reservoir quality in terms of porosity, types and distribution of reservoir fluids is based mainly on the evaluation of the shale volume. Therefore, qualitatively evaluating shaly sand requires an accurate estimate of the amount of shale (Soto Becerra, Arteaga et al. 2010).
The following are some of the clay indicators used to estimate shale volume from well logs.

V_{sh} From GR log

Gamma ray tool uses naturally emitted gamma ray radioactivity from the formation. The emitted gamma rays from the formation are counted at the gamma ray detectors. If no non-clay radioactive minerals are present and the level of radioactive clay is constant, the gamma ray reading can be expressed as a linear function of clay content as follows

$$I_{GR} = \frac{GR_{log} - GR_{sand}}{GR_{shale} - GR_{sand}} \qquad \text{Equation 2.1}$$

where,

GR_{log} = Gamma ray reading tool in the zone of interest

GR_{sand} = Gamma ray reading in clean zone or interval

GR_{shale} = Gamma ray reading in shale interval.

Equation 2.1 overestimates the clay volume in a clean interval (sands) rich in radioactive minerals other than shale (Poupon, Clavier et al. 1970), particularly true for radioactive sands and dolomite (Kamel and Mabrouk 2003). The gamma ray parameter is correlated as a linear relationship to shale volume. However, shale in a reservoir can be distributed in different ways such as laminated, dispersed and structural. Because of this distribution gamma ray responses will vary depending on the geometry of shale in the sand (Thomas and Stieber 1975).

Because of overestimating of shale volume by this technique for the presence of non-clay radioactive minerals, some early workers developed non-linear models such as Larionov, Clavier, and Stieber as illustrated in **Figure 6**. These methods are based on specific geographic areas or formation age to correct the shale volume estimated from linear relationship gamma (Kukal and Hill 1986). All these models are optimistic the fact that they yield shale volume that is lower than that given from linear gamma ray. Radioactive black organic materials in carbonate reservoirs cause an overestimation of shale volume from these methods (David, Rodolfo et al. 2015).

The use of linear and non-linear to estimate the shale volume of the reservoir depends on the way the minimum and maximum values are defined in the sand line and shale line respectively. The sand line and shale line may have one GR value in some parts but differs in some deeper level of the well. In all situations, the inaccurate calculations of shale volume influence the formation porosity and water saturation and consequently affect the original of oil in place or reserves.

Example of shale volume corrections as a function of Gamma Ray Index (I_{GR}) developed by Larionov (1969) for Tertiary Rocks.

$$V_{sh\ Larionov\ Tertiary\ Rocks} = 0.083(2^{3.71I_{GR}} - 1) \qquad \text{Equation 2.2}$$

where,

V_{sh} = shale volume

I_{GR} = Gamma ray index and is given by Equation 2.1

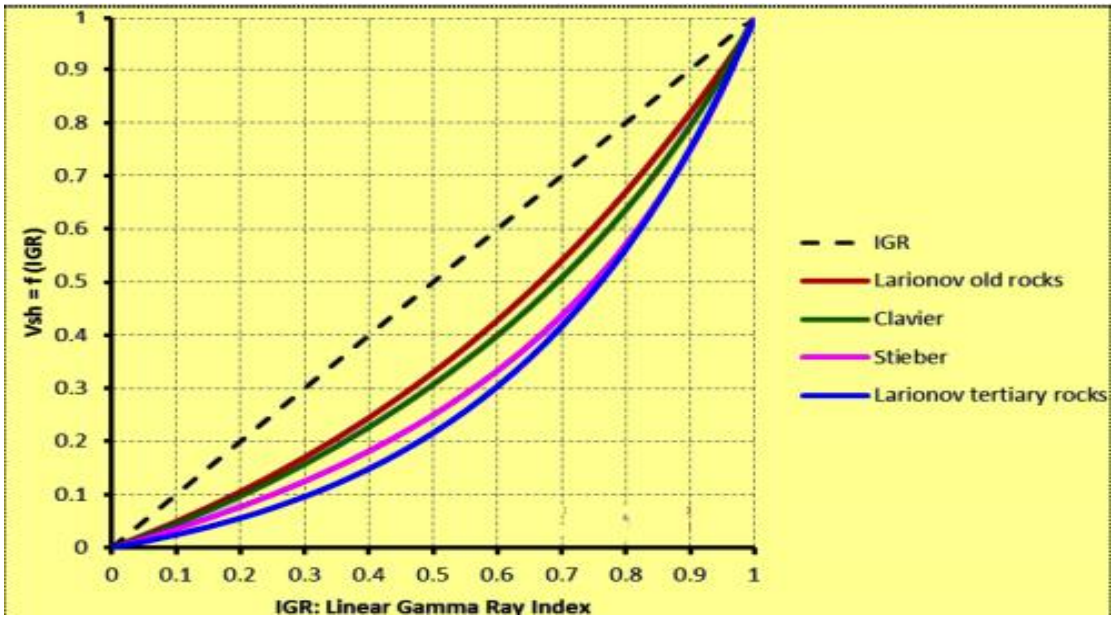

Figure 6: V_{sh} as a function of IGR (David, Rodolfo et al. 2015)

V_{sh} From Neutron and Density logs

The neutron and density porosity logs are common techniques and straightforward method for estimating the shale volume of the reservoir (Bhuyan and Passey 1994). The estimation of the volume of shale basing of naturally occurring gamma ray frequently overestimates the shale volume when encounters radioactive sands as sands will appear as shaly. From this consequence, the volume of shale estimated from neutron-density curves yields

more accurate shale volume. However, the presence of gas or light hydrocarbon in the reservoir makes this method is pessimistic (Adeoti, Ayolabi et al. 2009).

Gas in the formation affects neutron reading considerably by reducing the neutron porosity values due to low hydrogen index of the gas. On the other hand, clay or shale cause neutron reading increases dramatically making neutron apparent porosity too high. The effect of shale on density log depends on the density of shale present in the formation.

The neutron-density Equation can be written as follows

$$V_{\text{sh neutron}-\text{density}} = \frac{\emptyset_N - \emptyset_D}{\emptyset_{NSH} - D_{DSH}} \qquad \text{Equation 2.3}$$

where,

$\emptyset_N$= Neutron porosity in sand

$\emptyset_D$= Density porosity in sand

$\emptyset_{NSH}$= Neutron porosity in adjacent shale

$\emptyset_{DSH}$= Density porosity in adjacent shale

2.2.2 Porosity Estimation (Ø)

Porosity is the fraction of the pore space that is not occupied by the rock matrix. Porosity is one of the key parameters used to estimate the initial hydrocarbon in place. Any wrong calculation in porosity can translate directly to an error in volume estimation (Anyaehie and Olanrewaju 2010). There are various types of porosity being recognized within the petroleum industry. Only two types are mainly considered in use, which are effective porosity and total porosity.

Total porosity is defined as the fraction of the bulk volume of reservoir rock that is not occupied by fluid and Effective porosity is defined as the total porosity subtracting clay bound water (Gimbe, 2015).

Porosity Types and Determination

Porosity can be determined from direct measurements (neutron) or can be calculated from various logs eg. neutron and density, sonic, density, and NMR logs (standalone). Or can be obtained from the combination of logs eg. neutron and density logs. On the other hand, porosity can be obtained from laboratory measurements on cores samples.

Effective porosity (PHIE) from neutron and density logs

Density and neutron logs are two common physical measurements used in the formation evaluation. Because of their combined applications such neutron-density overlay, neutron-density crossplot they are widely used in determining lithology, estimating porosity and detecting gas zones from their crossover (Mao 2001). The neutron-density combination is still often the most reliable technique to estimate formation porosity from well logs. However, inaccurate characterization of matrix yields less accurate porosity and saturation estimates especially in complex lithology (Ijasan, Torres-Verdín et al. 2013).

In gas-bearing formation neutron porosity and density porosity are not equal caused by opposite effect the gas has on both tool's responses (Quintero and Bassiouni 1998). Like water, hydrocarbons contain hydrogen but at variable concentration which basically depend on the density of hydrocarbon in the reservoir. Practically, some oil has the same hydrogen as in water; gas on the other hand gas or light hydrocarbon has considerable lower hydrogen concentration and density as the result gas or light hydrocarbon have much effect on both density and neutron logging tool's responses (Gaymard and Poupon 1968). The presence of gas or light oil in the reservoir, a density-neutron technique underestimates the formation porosity and therefore effects on saturation and initial hydrocarbon in place volume.

The properties of shaly sand will have an influence on the behavior of the neutron reading. Shale is the rock that includes clay minerals containing bound hydrogen in the form of hydroxyl (OH-) as part of their structures. The bound hydrogen in the hydroxyl will affect the same way as hydrogen in water and hydrocarbon in pores. The neutron apparent porosity in shaly formation will

increase slightly from expected trend due to extra hydrogen in the hydroxyl group associated with clay minerals in shale (Ellis, Case et al. 2004). The effects of shale on density tool greatly depend on the density and type of clay minerals.

Porosity from Density Magnetic Resonance (DMR)

The presence of gas in the formation affects both nuclear magnetic resonance and density tools. The low proton density and insufficient polarization of gas cause a reduction in the nuclear magnetic resonance signal strength and the apparent porosity is underestimated. The density porosity, however, is overestimated because of the low gas density. The porosity of the clean liquid phase-bearing formation can be accurately quantified from either NMR or the density logging tools. The presence of gas phase both tools are significantly altered causing porosities to deviate from the formation porosity (Thern and Chen 1999).

Density-magnetic resonance (DMR) is the new method for evaluating gas-bearing reservoir. The method combines total porosity from combinable magnetic resonance tool (TCMR) and density-derived log porosity (DPHI) and the method is referred to as Density-Magnetic Resonance method. The NMR gas-corrected total porosity provides more accurate hydrocarbon volume estimates (gas reserves) (Freedman, Minh et al. 1998).

This method provides some advantages over the traditional method (neutron-density method), NMR logging tools are sensitive to only hydrogen present in the pores of the fluid and not affected by mineralogy; neutron tools are sensitive to all hydrogen includes those form part of the clay matrix and those due to hydration. Scatters and absorbers such as chlorine and other elements affect the neutron tool (Kleinberg and Vinegar 1996). The use of neutron-density logs for gas detection is not always reliable because shale and thermal absorbers can suppress the crossover effect (Freedman, Minh et al. 1998).

The Equation for gas corrected total formation porosity is given below

$$\emptyset = \frac{\mathrm{DPHI} * \left(1 - \frac{(\mathrm{HI})_g * P_g}{(\mathrm{HI})_f}\right) + \frac{\lambda * \mathrm{TCMR}}{(\mathrm{HI})_f}}{(1 - \frac{(\mathrm{HI})_g * P_g}{(\mathrm{HI})_f} + \lambda} \qquad \text{Equation 2.4}$$

Equation 2.4 above is the gas-corrected total porosity and is the weighted sum of DPHI and TCMR / $(HI)_f$ and has the form of

$$\emptyset = \text{DPHI} * w + (1 - w) * (\frac{\text{TCMR}}{(HI)_f} \qquad \text{Equation 2.5}$$

where the weight is given by

$$w = \frac{1 - \frac{(HI)_g * P_g}{(HI)_f}}{(1 - \frac{(HI)_g * P_g}{(HI)_f} + \lambda} \qquad \text{Equation 2.6}$$

A good approximation of Equation 2.5 is set w≅0.6, (1-w) ≅ 0.4 and $(HI)_f \cong 1$, w can be verified by using typical values of parameters (Freedman, Minh et al. 1998). From this approximation equation 2.5 can be reduced to

$$\text{DMRP} \cong 0.6 * \text{DPHI} + 0.4 * \text{TCMR} \qquad \text{Equation 2.7}$$

where,

∅= total formation porosity

$(HI)_g$= hydrogen index of gas at reservoir conditions

$(HI)_f$= hydrogen index of the liquid phase in the flushed zone at reservoir conditions.

$P_g \equiv 1\text{-exp } (-\frac{W}{T_{1,g}})$=gas polarization function.

W= wait time for CPMG pulse sequence

$T_{1,g}$= gas longitudinal relaxation time at reservoir conditions.

λ Is the parameter that is proportional to the density difference between the gas and liquid phases and is responsible for gas effect on the density log.

2.2.3 Water Saturation (S_w)

Water saturation is the fraction of the pore volume occupied by a certain fluid. Determination of water saturation is one of the important parameters in formation evaluation from which initial oil in place can be calculated, which depend on the volume of the reservoir, porosity, and water saturation (Fleury, Efnik et al. 2004). In petrophysical formation evaluation, water saturation can be calculated from different saturation models depending on whether the reservoir is clean or shaly.

Water saturation models in shaly sand hydrocarbon reservoirs are the expansion of the Archie equation with the extra term to accommodate the volume of shale and their associated electrical properties.

There are many shaly sand interpretation models that are often used today because no uniquely satisfactory results have been reached (Doveton 2001).

The following Equations or Models are mostly used today to evaluate the hydrocarbon reservoirs depending on shale contents and characteristics of the reservoir.

The Archie Equation/Model

The electrical log interpretation for evaluation of hydrocarbon saturated permeable formation is based on Archie's equation, which relates the water saturation to formation water resistivity, porosity and resistivity of saturated formation (Alfosail and Alkaabi 1997). However, the use in a quantitative evaluation has limitation due to various factors that tend to obscure its reading obtained (Archie 1942).

This relationship is given by the following Archie's Equation.

$$S_w{}^n = \frac{a * R_w}{\emptyset^m * R_t} \quad \text{or} \quad S_w = \sqrt[n]{\frac{a * R_w}{\emptyset^m * R_t}} \qquad \text{Equation 2.8}$$

where,

a= tortuosity of the rock

m= Cementation exponent

n= saturation exponent

Ø= Porosity

S_w= Formation water saturation

R_w= Resistivity of formation water

R_t= Formation resistivity

Archie's equation was specifically established for clean sands and does not take into account the clayey materials (Worthington 1985). In a clean formation, the matrix is an electrical insulator such that only fluids in the pores of the formation have the ability to conduct electrical current. In shaly sand formations the determination of water saturation is the more complicated task; shale constitutes a part of the rock matrix and is able to conduct electrical current and consequently influence on rock resistivity, and complicate log interpretation (Bhatt, Helle et al. 2001); (Poupon, Loy et al. 1954).

Archie assumed that the rock matrix is nonconductive. However, clay materials in sandstone add conductivity enough to influence the Archie derived water saturation values from being high and therefore pessimistic for potential hydrocarbon reservoir (Doveton 2001). In shaly sand formation, Archie equation is less applicable and therefore other modified models (shaly sand saturation models) have to be applied to estimate hydrocarbon saturation of the reservoir. These models take into account of shale's conductivity as an additional term to the origin Archie's equation. The conductivity of shaly saturation models is given by the following general equation:

$$C_t = C_w/F + C_{sh} \qquad \text{Equation 2.9}$$

where,

C_t = total formation conductivity

C_w = conductivity of formation water

F = formation factor

C_{sh}= conductivity of shale

The Indonesian Model (Poupon and Leveaux Model)

The model was developed for shaly sand interpretations and consists of two media occurring in alternating layers, the two layers are clean sand and shale laminae (Fertl and Hammack 1971). The model is used for calculating effective water saturation in shaly sand formations and is independent of the shale distribution in the reservoir (Bhatt, Helle et al. 2001).

The relationship between the formation resistivity and the formation parameters affecting it (includes R_w, R_{sh}, S_w, and V_{sh}) was proposed by (Poupon and Leveaux 1971) and is given by the following equation.

$$\frac{1}{R_t} = \frac{(V_{sh})^c S_w}{R_{sh}} + \frac{\emptyset^m {S_w}^n}{aR_w} \qquad \text{Equation 2.10}$$

where,

m and **n** are cementation and saturation exponents respectively and exponent **c** is usually taken to be 1, sometimes larger values up to 2 may be used, R_t true resistivity of formation from deep resistivity log, R_w formation water resistivity at formation temperature, V_{sh} volume fraction of shale in the formation, R_{sh} is the resistivity of the shale.

Equation 2.10 above appeared to overestimate the water saturation when the ratio of R_{sh}/R_w was low and shale fraction in the formation is higher. Equation 2.11 below provided more accurate S_{we} results.

$$\frac{1}{\sqrt{R_t}} = \left(\frac{V_{sh}^{\left(1-V_{sh}/2\right)}}{\sqrt{R_{sh}}} + \frac{\emptyset^{\frac{m}{2}}}{\sqrt{aR_w}} \right) S_{we}^{\,n/2} \qquad \text{Equation 2.11}$$

Both Equations 2.10 and 2.11 rely on the accurate estimation of formation parameters (formation porosity, formation water resistivity, and amount of shaliness) to give more satisfactory water saturation results. In fact, the Indonesian equation was developed for use in Indonesia because there comparatively fresh water formation and high degree of shale contents which are shortcomings of the other equations and has subsequently found to be applicable in other areas (Worthington 1985).

The Simandoux Model

The experiment studies by the Simandoux on artificial homogeneous mixtures of sand and clay (montmorillonite) have suggested that the conductivity (resistivity) can be expressed by the following relationship (Worthington 1985); (Fertl and Hammack 1971).

$$\frac{1}{R_t} = \frac{\emptyset^m}{a\,R_w} S_w^{\,n} + \frac{V_{sh}}{R_{sh}} \qquad \text{Equation 2.12}$$

And its modified form is (Modified Simandoux Equation).

$$\frac{1}{R_t} = \frac{\emptyset^m \,.\, S_w^n}{a\,R_w(1-V_{sh})} + \frac{V_{sh}\,.\,S_w}{R_{sh}} \qquad \text{Equation 2.13}$$

R_{sh} = Resistivity of dispersed clay.

2.2.4 Permeability (k).

Rock permeability is one important flow parameter associated with subsurface production and injection; it is an intrinsic characteristics of the materials that determines how easily the fluids can pass through it (Ahmed, Crary et al. 1991). The parameter of significance is reflected by the number of sources (well logs, cores and well testing) and among others are used to estimate rock permeability (Lin and Salisch 1994).

Darcy`s equation is extensively used in petroleum engineering to determine the fluid flow through permeable materials. Permeability measurement unit is darcy where $1D=0.9869*10^{-12}m^2$. For 1 unit of darcy is the permeability of a unit volume of sand at a pressure differences of $1dyne/cm^2$ between ends of the sample that causes a fluid with a dynamic of 1 poise to flow a rate of $1cm^3/s$ (Gimbe, 2015).

$$Q = k\frac{A_t\,\Delta P}{\mu L} \qquad \text{Equation 2.14}$$

where,
Q = volumetric flow rate in m^3/s through a porous medium with a cross-section area of A_t perpendicular to the direction of flow.
k=permeability in (mD)
μ= dynamic viscosity of the fluid (centipoises)
ΔP= pressure drop across the porous medium of length (L). **Figure 7** gives the definition of Darcy`s law.

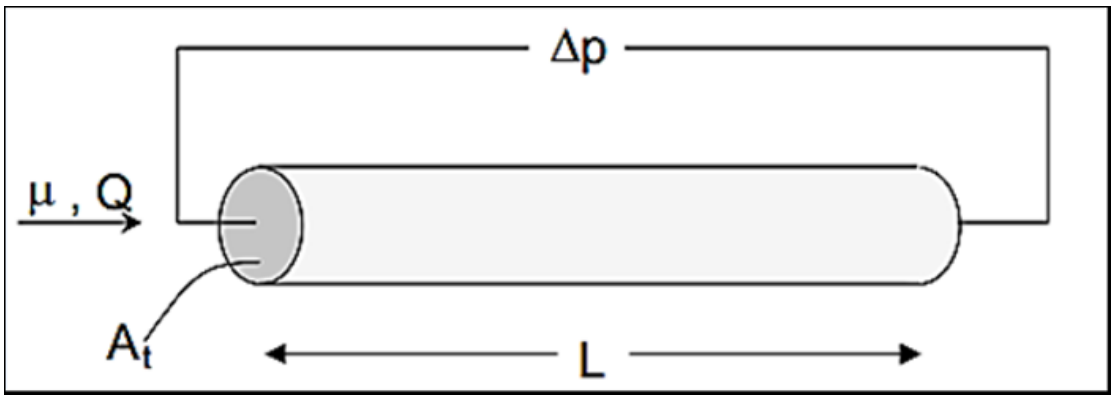

Figure 7: Definition of Darcy`s law (Gimbe, 2015)

Permeability Determination

Estimation of permeability from well logs has a particular advantage of the economy due to their continuity measurements. In fact, permeability is a complex parameter to determine because is affected by many factors such as size of the matrix grain, type, amount and distribution of clay minerals, porosity, and many other factors.

There are a large number of equations and techniques exist for estimating formation permeability from well logs and none of these is universally applicable from field to field, well to well, or even from zone to zone without making adjustments of the constants (Coates and Dumanoir 1973).

In normal reservoir, permeability can be accurately estimated from porosity because of good relationship that exists between porosity and permeability of these reservoirs. Poor correlation between porosity and permeability exists in tight sandstone reservoirs because of heterogeneity posed by shales (Xiao et al., 2014).

Generally, there are two models that are used to estimate permeability from nuclear magnetic resonance data. The Coates model that uses the ratio of the irreducible water to free water determined by a T_2- cutoff and the Shlumberger

Doll- Research model (SDR) that uses the log-mean of the relaxation spectrum (McCarney, Butler et al. 2015)

Timur Coates model (TIM)

$$k_{T-C} = \left(\frac{\emptyset}{C}\right)^{m} * \left(\frac{BVM}{BVI}\right)^{n} \qquad \text{Equation 2.15}$$

Schlumberger Doll Research Centre (SDR) model

$$k_{2GM} = C\emptyset^{a}\, T_{2GM}^{b} \qquad \text{Equation 2.16}$$

where,

K= permeability (mD)

Ø = porosity (%)

T_{2GM} = is the logarithmic mean of NMR T_2 spectra (ms).

MVB= free fluid volume (%)

BVI= bulk volume irreducible (%)

A, b, C, m, and n are constants.

These are empirically derived equation based upon specific rocks and fluid data sets. The successful application of these models demands a constant C and partition of free fluid fraction for Timur- Coates models (Tyurin, Borghi, Gossenberg, Pirrone, & Cominesi, 2015).

3. METHODOLOGY

Formation evaluation was performed using a composite of well logs (Gamma ray, Neutron, Density logs, Resistivity, Nuclear Magnetic Resonance log, and Elemental Capture Spectroscopy). The well logs used in the study were supplied by the Norwegian University of Science and Technology (**NTNU**) and was acquired by **STATOIL** in the Southern Barents Sea (well 7220/8-1). **Figure 8** and **Figure 9** shows the well logs used for the evaluation.

The task involves lithology and fluid interpretation (permeable hydrocarbon bearing zones, and fluids characterization) and quantification evaluation (shale volume, formation porosity, saturation, and permeability computation) from logs.

Lithology Identification

The Gamma-ray, ECS, and neutron-density cross plot were examined for lithologic discrimination. The GR which measures the natural radioactivity reflects clay contents in the formation. The separation between neutron porosity and bulk density logs was then used to characterize the particular lithology type. The neutron-density cross plot was then used to discriminate the type of lithology and the information was combined with ECS log for complete lithologic characterization.

The resistivity log and Gamma ray logs were used to discriminate the potentially permeable pay and non-pay hydrocarbon bearing zones. The resistivity and Gamma ray log reflects high and low signature in permeable zones respectively and vice-versa reflects (**Figure 8**).

Fluid Identification and possible fluids contact estimation

Resistivity logs, combined neutron and density logs were used to characterize and identify fluid types in the reservoir (hydrocarbon and non-hydrocarbon bearing zones).

The presence of gas in the reservoir results in large crossover between neutron-density logs as shown in **Figure 9** at the gas-bearing interval (1276.16-1312.64 m) when plotted in the same log scale. However, the presence of oils in the reservoir results in decreased separation between neutron porosity-bulk density log and an increase in resistivity readings. Differences in fluid densities, neutron-density separation varies and being large in gas and decreases through oil to water zones.

Resistivity logs were then used to identify the formation fluids (gas/oil/water) and possible fluids contact. Hydrocarbon bearing zones were indicated by high resistivity readings and decreases in water zones.

Shale Volume Estimation:

The shale volume ($\mathbf{V_{sh}}$) was calculated from equation 2.17 which utilizes the values of Gamma Ray (GR) in equation 2.18. Equations 2.17 and 2.18 are found in Schlumberger Techlog software.

$$V_{\text{sh Larionov Tertiary Rocks}} = 0.083(2^{3.71 I_{GR}} - 1) \qquad \text{Equation 2.17}$$

where,

V_{sh} = shale volume

I_{GR} = Gamma ray index and is given by the following Equation

The gamma ray index (I_{GR}) is estimated from the following relationship:

$$I_{GR} = \frac{GR_{log} - GR_{min}}{GR_{max} - GR_{min}} \qquad \text{Equation 2.18}$$

where,

GR_{log}= measured GR from log

GR_{min}= GR reading in the zone of interest

GR_{max}= maximum GR reading in the zone of interest

The corresponding values of GR_{max} and GR_{min} is 120API and 12API which were read in the clean and shale intervals respectively.

GR_{log} is directly supplied from the GR log.

Porosity Determination (∅)

Porosity for potential hydrocarbon-bearing zones was calculated from DMR (combined density derived porosity and total combinable magnetic resonance porosities) and combined neutron-bulk density porosity logs. The DMR method appears to be optimistic when compared to core-derived porosity (**Figure 11**), which was then used in saturation calculations. The combined neutron and density method underestimated the formation porosity in the gas-bearing interval (1276.16-1312.64 m).

The following equation was used to estimate formation porosity from density derived porosity and total combinable magnetic resonance (DMR), which gives the total corrected gas porosity.

$$DMRP = \cong 0.6 * DPHI + 0.4 * TCMR \qquad \text{Equation 2.19}$$

And DPHI is estimated density porosity formula

$$\text{DPHI} = \frac{\rho_{\text{matrix}} - \rho_{\text{log}}}{\rho_{\text{matrix}} - \rho_{\text{fluid}}} \qquad \text{Equation 2.20}$$

where,

DMRP = total corrected gas porosity

DPHI = density-derived log porosity

TCMR = total porosity from combinable magnetic resonance log from NMR log.

ρ_{matrix}= matrix density and was assumed to be 2.65 $^{g}/_{cm^3}$ (sandstone matrix)

ρ_{log}= formation bulk density $^{g}/_{cm^3}$, supplied from density log.

ρ_{fluid}= fluid bulk density and was assumed to be 1 $^{g}/_{cm^3}$.

The porosity from the **DMR** method was applied to all saturation models to calculate the average water saturation.

The effective porosity was estimated from a combined neutron and density logs available in Schlumberger Techlog 2015.3.

Water Saturation Calculation (S_w)

Water saturations of uninvaded zone were calculated from both clean Equation and shaly-sand saturation Equations.

Clean Saturation Equation

(i) Archie Equation

$$S_w{}^{n} = \frac{a * R_w}{\emptyset^m * R_t} \quad \text{or} \quad S_w = \sqrt[n]{\frac{a * R_w}{\emptyset^m * R_t}} \qquad \text{Equation 2.21}$$

Shaly sand Saturation Equations

(i) **Indonesian Equation**

$$\frac{1}{\sqrt{R_t}} = \left(\frac{V_{sh}^{\left(1-V_{sh}/2\right)}}{\sqrt{R_{sh}}} + \frac{\emptyset^{m/2}}{\sqrt{aR_w}} \right) S_{we}^{\,n/2} \qquad \text{Equation 2.22}$$

(ii) **Simandoux Equation**

$$\frac{1}{R_t} = \frac{\emptyset^m}{a\,R_w} S_w^{\,n} + \frac{V_{sh}}{R_{sh}} \qquad \text{Equation 2.23}$$

(iii) **Modified Simandoux Equation**

$$\frac{1}{R_t} = \frac{\emptyset^m * S_w^n}{a\,R_w(1 - V_{sh})} + \frac{V_{sh} * S_w}{R_{sh}} \qquad \text{Equation 2.24}$$

where,

a = turtuosity

m = cementation factor

n = saturation exponent

R_w = formation water resistivity

R_{sh} = shale resistivity

R_t = formation resistivity

S_w = water saturation

$\emptyset$ = formation porosity

Data Determination

Formation resistivity values (R_t) was directly supplied from deep Laterolog (RT_HRLT) of uninvaded zone. Similarly, the resistivity of shale (R_{sh}) was obtained from the same resistivity (deep resistivity) log in the shale zone and its value is 2.2 Ωm.

Formation water resistivity(R_w) at formation temperature was determined from two methods; from Archie Equation in the water zone and from precomputation available in Schlumberger Techlog software at formation temperature. From the Archie equation in the water zone the value of 0.037Ωm was obtained and was applied to all models in saturation calculations (clean and shaly models).

The value of cementation factor (**m**) and saturation exponent (**n**) was assumed to be 2 and the tortuosity (**a**) was assumed to be 1.

1st Case: Clean Hydrocarbon Interval

Considering only the clean (sand) hydrocarbon-bearing zone (**Zone_4**). The average water saturations were calculated from all equations above (2.21, 2.22, 2.23, and 2.34) assuming the same model parameters (**m**, **n**, and **a**) and the results of these calculations are presented in **Tables (1** through **4).**

2nd Case: Entire Hydrocarbon Interval

The second water saturations were calculated from all saturation models (2.21, 2.22, 2.23, and 2.34) for the entire potential zones applying the same parameters. The results of these calculations are presented in **Tables (5** through **8)**.

To obtain the average water saturation (S_w), shale volume, porosity, and water saturation cutoff values were applied on three different flags (Rock, Reservoir, and Pay). The following cutoff values were used:

V_{sh}<=0.45 (fraction)

∅>=**0.1**(fraction)

S_w<=0.6 (fraction)

Net Pay

The net pay is the thickness that contains economically productive interval. It was determined by applying cut-offs to rock properties. The reservoir interval was defined by applying the porosity of greater than 10% and shale volume of less than 45%. Water saturation cut-offs value of 60% was used. The net pay was considered to contain hydrocarbon if the S_w<=60% within the reservoir.

Hydrocarbon Pore Thickness (HCPOR-TH)

This was calculated from Schlumberger Techlog software. Applying the same cut-offs as stated above. $\text{HCPOR} - \text{TH} = \text{average porosity} * (1 - S_w) *$ net thickness.

Permeability Estimation (k)

Formation permeability (k) was estimated from two models (Timur-Coates) and the Schlumberger-Doll-Research model (SDR).

Timur-Coates model (KTIM)

$$k_{T-C} = \left(\frac{\emptyset}{C}\right)^{m} * \left(\frac{BVM}{BVI}\right)^{n} \qquad \text{Equation 2.25}$$

Shlumberger-Doll-Research Centre (SDR) model

$$k_{2GM} = C\emptyset^{a}\, T_{2GM}^{b} \qquad \text{Equation 2.26}$$

where,

k= permeability (mD)

Ø = porosity (v/v)

T_{2GM} = Geometrical mean of NMR T_2 spectra (ms).

FFV= free fluid volume (%)

BFV= bound fluid volume (%)

C, m, n, a, and b are constants.

Both log-derived permeability and core permeability are shown in **Figure 11.**

Porosity exponent (a and m) were assigned to be 4

Phi Ratio exponent (n) and T_2 exponent SDR (b) were assigned to 2.

4 QUALITATIVE INTERPRETATION

Well logs have many applications in formation evaluation including lithology and fluid identification and many other applications can be obtained them. These logs can be used as the single log (eg. GR log) or combined logs (eg. neutron and density logs) to give information about lithology and fluid types contained in the reservoir. **Figure 8** and **Figure 9** shows the composite logs used in the lithology and fluid identification.

4. 1 Lithology Identification

The lithology identification penetrated by any well involves a combination of different logging curves. The following logs are used to identify the lithology; the Gamma ray, Neutron and density logs, and elemental capture spectroscopy (ECS). Based on log response the whole interval is divided into six zones.

Zone_1, the zone is marked by elevated gamma ray (track 1) and a large separation between neutron and density curves (track 2). The ECS which responds to mineral fraction shows high clay fraction (shale) relative to quartz (sand) in track (5) of **Figure 8**. Plotting the data points of Zone_1 on the neutron-density cross plot with the gamma ray as a color scale most of the data points fall in the shale zone (lower region) of the cross plot Appendix A1. Based on the observation made above, Zone_1 suggests being a shale zone with no potential to be a hydrocarbon bearing zone.

Zone_2, the identification of the zone is supported by relatively low gamma ray reading (track 1), the crossover between neutron and density curves which suggests for the change of lithology and fluid types in the formation and relatively low clay contents from ECS (track 5). The neutron-density cross plot technique is then used to confirm the lithology type as shown in Appendix A2. Most of the data point clouds on the sandstone line (quartz) and some are scattered and fall below and above the sandstone line. The color scale suggesting

the presence of radioactive materials (shale) and non-radioactive materials (carbonate and pyrite) as depicted on ECS curve in track 5. From this observation, Zone_2 suggests being the shaly sand zone. This zone falls within the Stø Formation and is the hydrocarbon-bearing reservoir.

Zone_4, the zone is marked by the relatively lower gamma ray and small to almost no clay contents as shown on ECS log. Most of the data points clouds on the sandstone line of the neutron-density cross plot as shown in Appendix A3. Combining these observations, the zone is confirmed to be a clean sandstone interval in the Stø Formation.

Zone_5 and **Zone_7** are similar to **Zone_2** displaying the same log characteristics with small negative separation between neutron and density curves and relatively low gamma ray reading. With an exception of the interval (1375-1380 m, Zone_6) which is characterized by high gamma ray signature and high clay fraction as shown on the ECS log curve suggesting a shale interval. This zone correspond with Appendix A4 of the neutron-density cross plot.

The cross plots confirm that the Formations are the mixture of sand, shale and limestone (cemented carbonated). The presence of carbonate in zones is probably the cause of high-density peaks accompanied by low neutron porosity readings and high resistivity readings. It therefore that the well penetrated sand (sandstone) mixed with clays (claystone) and some cemented carbonate (siderite) and pyrite.

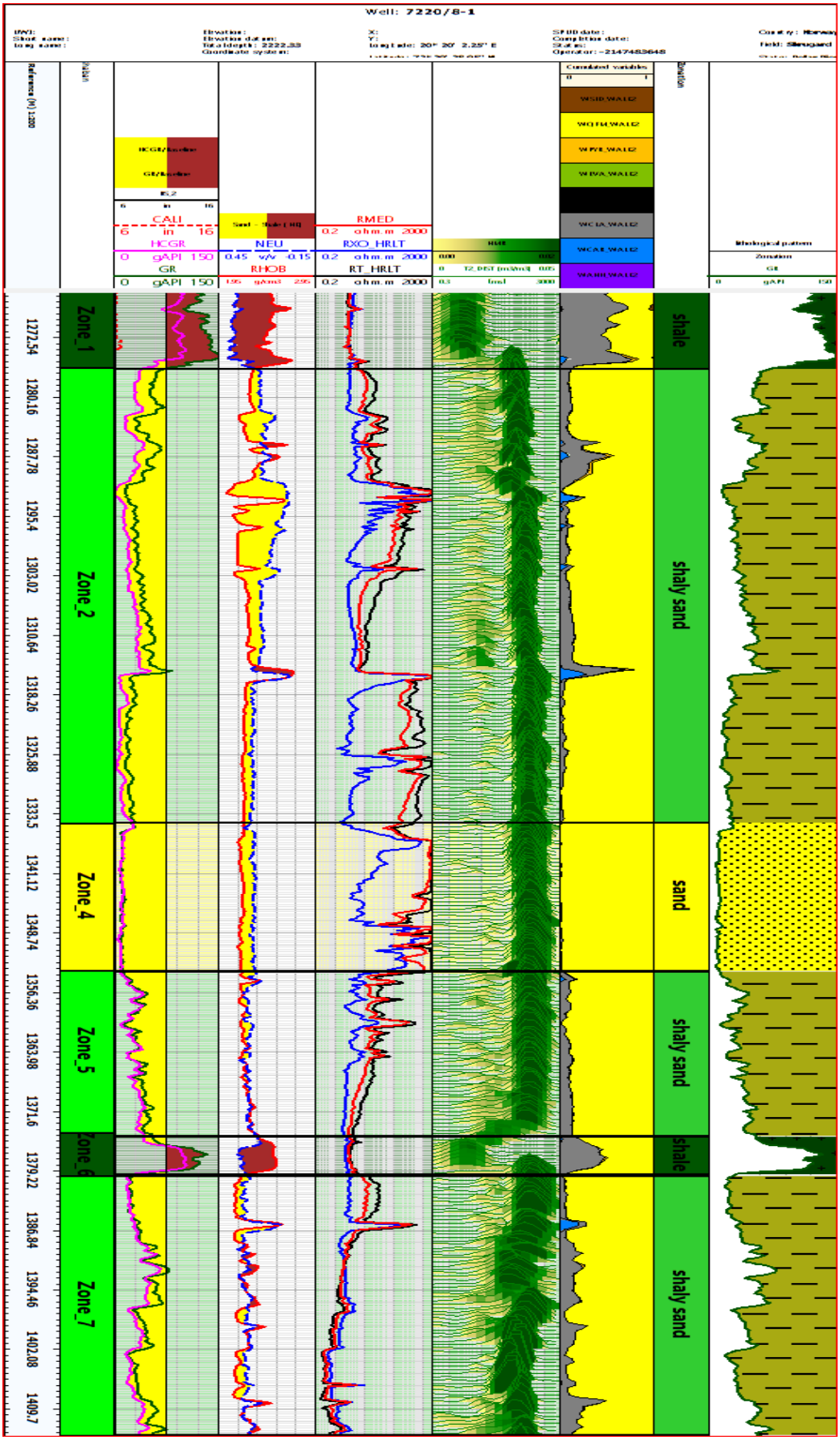

Figure 8 : Lithology identification from well logs

4.2 Fluid Identification

Availability of gamma ray, resistivity, neutron, and density logs in the study area enabled the reservoir and its contained fluid to be easily identified on logs. Resistivity and neutron-density logs have different response characteristics on different fluid types.

The resistivity logs are characterized by higher resistivity readings than the adjacent shale. The large crossover between neutron-density curves in Zone_A is the reflection of the hydrocarbon-bearing gas interval (1276-1312 m). The presence of clays in the interval may cause a slight reduction in formation resistivity values. There is also higher abnormally resistivity readings within the interval which might be caused by the presence of cemented carbonate or heavy minerals strikes within the porous shaly sand.

The even higher resistivity readings accompanied by the minor crossover separation between neutron and density suggesting oil-bearing Zone_B (1312-1395 m). The same reason explained above for higher abnormally resistivity values in some secrete interval.

The water zone (Zone_C) is marked by decreased resistivity readings and neutron and density separation. The small separation between all resistivity curves may be due to small contrast between formation water resistivity and mud filtrate used.

Resistivity logs were then used to identify the formation fluids (gas/oil/water) and possible fluids contact. Hydrocarbon bearing zone is indicated by high resistivity readings and decreases in water zone. This information is combined with neutron-density curves to predict the possible fluid contacts as indicated in **Figure 9.**

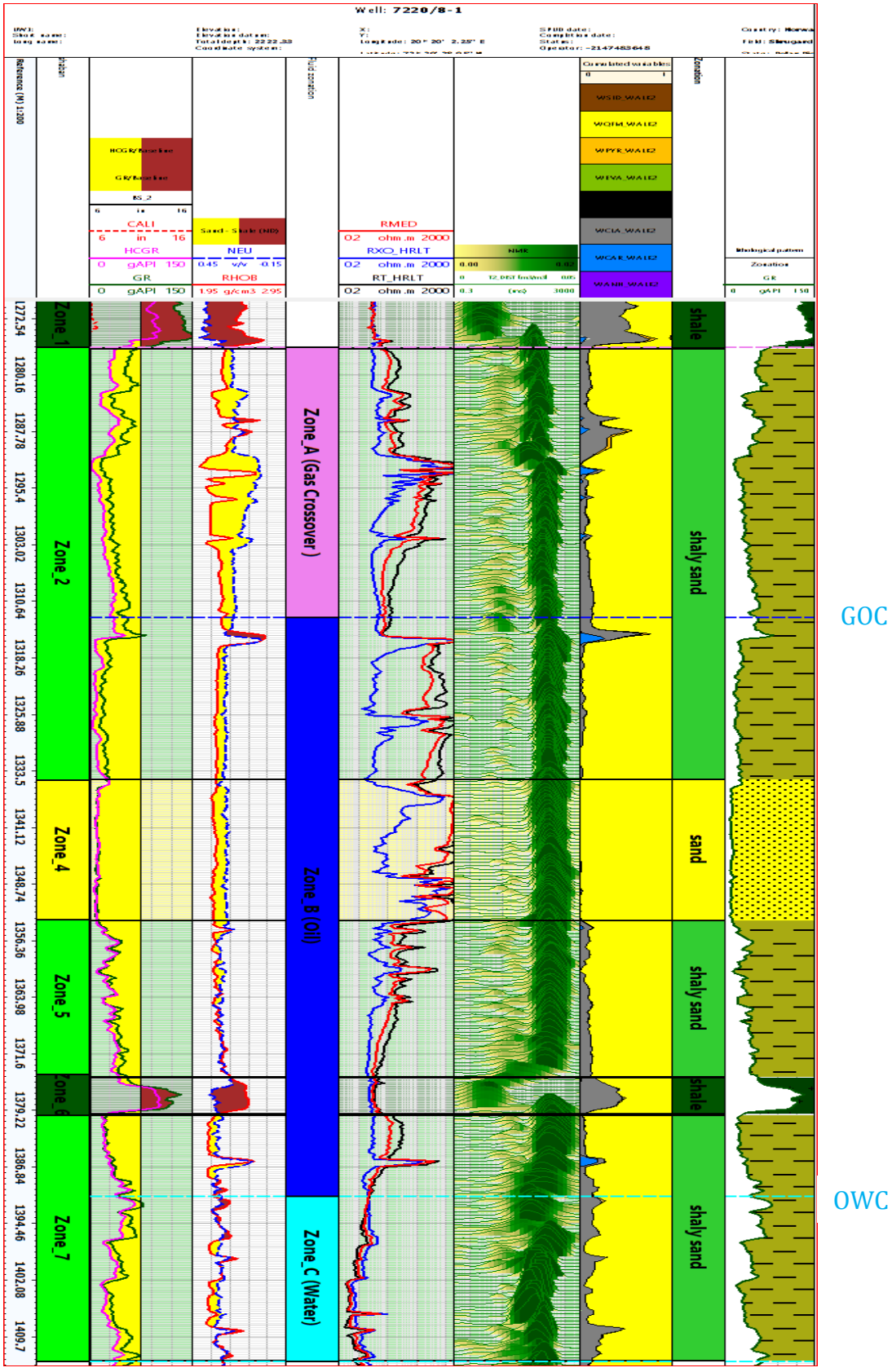

Figure 9: Fluid identification and fluid contacts estimation from well logs

6 RESULTS AND DISCUSSION

The use of log signature and neutron-density cross plot has identified that the Stø and the Nordmela Formation where the well 7220/8-1 was drilled is dominated by sandstone (sand) with minor amount of shale or clays (**Figure 8**) and **Appendix A**. When the data points are plotted on neutron-density cross plot most of them clouds on the sandstone line with few disperses toward the limestone line and shale region. The neutron and density cross plot have revealed the presence of thin cemented carbonate where siderite and pyrite are identified from ECS log. Appendix A (1 through 4) shows the illustration of lithology for each zone.

Figure 10 shows the shale distribution within the entire reservoir interval penetrated by the well (7220/8-1). Most of the data points lie (clouds) along the shale and clean sand line indicating laminated shale type of distribution. Some point scatters toward the dispersed shale point which indicates that the formation is associated with a few amount of dispersed shale within the porous sand reservoir. **Appendix C (**1 through 4**)** shows the shale distribution for each zone as marked in **Figure 8** with Zone_1 and Zone_6 being excluded but included in **Appendix C5**. From various literatures, it is said that even small amount of dispersed shale may have a large impact on reservoir quality and on shaly-sand saturation interpretation models.

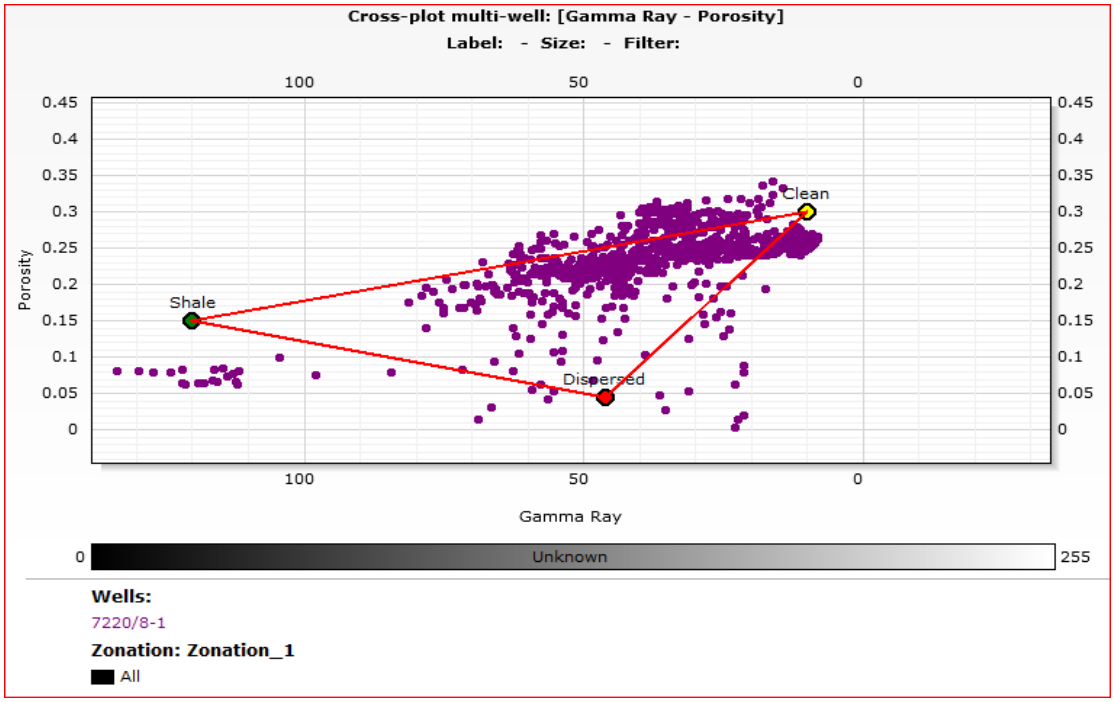

Figure 10: Shale distribution in sandstone for the well 7220/8-1

The comparison of calculated shale volume from all V_{sh} equations is shown in **Appendix B 1**. The result shows that the shale volume calculated from standard linear GR and N-D methods are relatively higher as compared to nonlinear method (Larionov for Tertiary rocks). The overestimation of shale volume by linear GR method can be contributed by the presence of non-clay radioactive minerals such as micas, feldspars. Moreover, this method assumes a linear relationship between shale volume and gamma ray reading. The nonlinear model which is based on specific geographical area and age of the rocks basically correct the shale volume from linear GR method.

The computation of the shale volume from both linear and nonlinear equations depends on defining the minimum (sand) and maximum (shale) lines.

Calculated shale volume computed from neutron-density logs is again higher than nonlinear GR method. The fact is, formation gas affects both neutron porosity and bulk density logs. The neutron porosity is underestimated due to low hydrogen concentration and the density porosity is overestimated because of the low formation gas density. In gas-bearing interval (1282.446-1303.02 m) the calculated shale volume from this method is underestimated (gas effect).

Therefore, the nonlinear GR method produced the lowest shale volume and ultimately used in effective porosity and saturation calculations.

Formation Porosity (Ø)

Porosity is the fraction of voids of the total volume of the rock. There are many equations often used to estimate either effective or total porosity from well logs. In this study, two methods are selected to calculate formation porosity; the first being N-D method (combined neutron-density porosity logs) and the second being a DMR method (combination of density derived porosity and combinable total magnetic resonance porosities)

Appendix B2 compares the formation porosity calculated from both models and **Figure 11** compares the log-derived porosity with the core porosity. The underestimation of porosity over the gas zone (1276.16-1312.64 m) by the neutron-density technique is that this method relies on the neutron and density logs to deliver the effective porosity.

Light hydrocarbons or gas-bearing formation makes a difference in neutron porosity and density tools response. The low hydrogen concentration of gas leads to low neutron porosity values. On the other hand, apparent density porosity is overestimated due to low gas density. Shaliness in the formation may again influence the effective porosity from neutron and density logs. The nature and their associated bound water of the clay minerals have an influence on neutron tools response by increasing the apparent neutron porosity. But, their effect depends on clay mineral type available in the formation.

The even more accurate porosity has been obtained by the Density Magnetic Resonance porosity method. This method appears to give a reliable estimate over the traditional technique (neutron and density logs) in the gas interval.
It is worth mentioning that uncertainties in the model parameters may affect the final results for both methods.

In clean oil or water-bearing zone (1318.26-1371.6 m) both methods give a relatively good agreement (**Appendix B2**). The underestimation of the effective porosity by the neutron-density technique can be checked against core-derived porosity (**Figure 11**) when plotted in the same log scale. The calculated porosity from the DMR method shows a relatively good match with the core in the gas interval. The effective porosity from the combined neutron and density logs is underestimated to some extend in the gas-bearing interval. The average porosity from the neutron-density and the DMR are 18.87% and 22.04% respectively in the gas zone where the average core porosity in the gas zone is 25.38%.

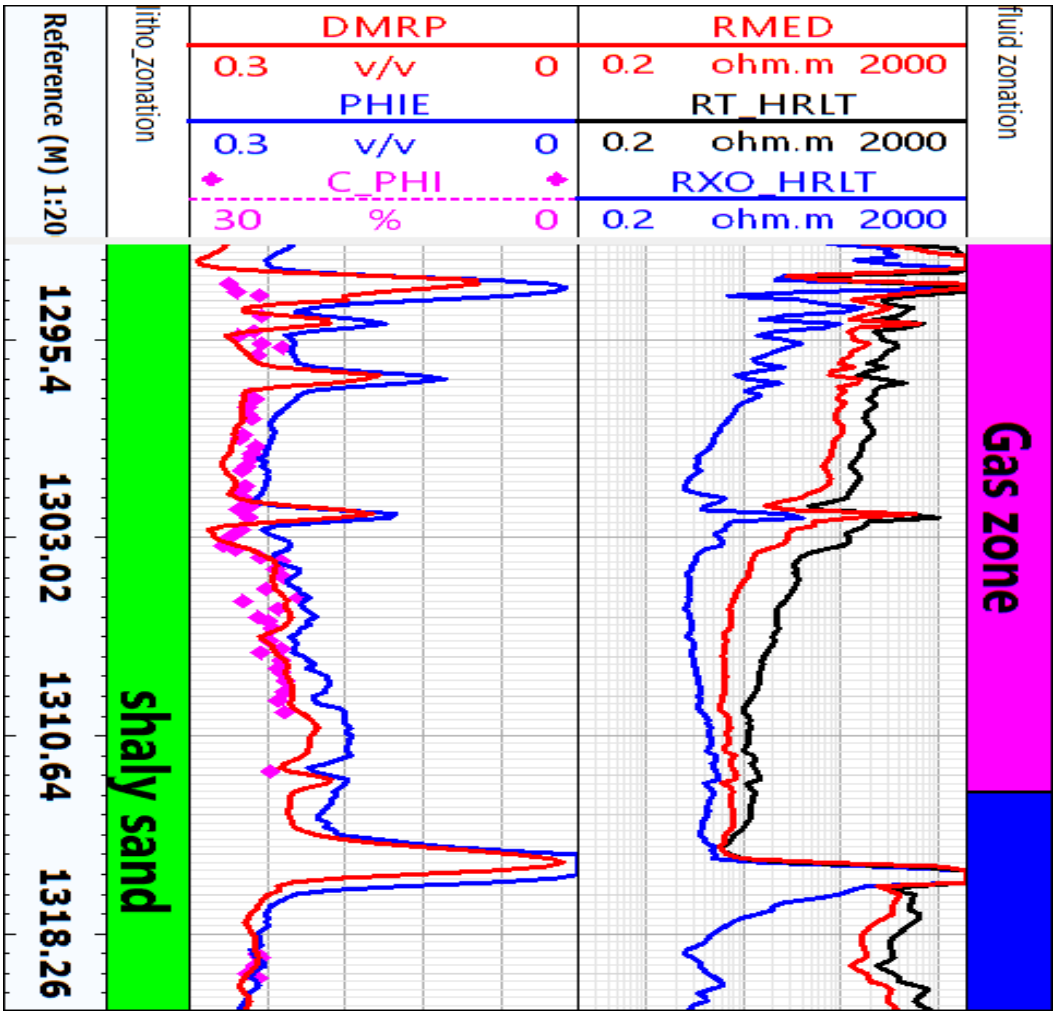

Figure 11: comparison of DMRP (red curve), N-D (blue curve) logs with core-derived porosity (pink diamond)

Water Saturation (S_w)

Water saturation is the fraction fluid of the pore volume occupied by water. The ultimate of any petrophysical analysis and evaluation is to compute water saturation in the reservoir. Because the economic production decisions of hydrocarbon from a potential reservoir mainly depend on rock water saturation. Furthermore, it is an important component in determining the hydrocarbon saturation (1-$\boldsymbol{S_w}$**)** or the original oil in place (OOIP) and original gas in place (OGIP).

Determination of water saturation (S_w) from well logs is very challenging because there many equations available to deliver it. Unfortunately, there is no unique equation for shaly models accurately estimate it expect for the clean reservoirs in which Archie`s equation have proved successfully. In shaly-sand reservoir, each equation tend to produce different water saturation values due to varying amount, distribution, and the associated bound water of shale or clays.

For this study, the reservoir is evaluated using four different saturation equations (clean and shaly-sands) which includes Archie, Indonesian, Simandoux, and Modified Simandoux. It is worth emphasizing that each of these equations is differently affected by shale as explained above in additional to model parameters.

In shaly-sand reservoir, the Archie model often overestimates the water saturation as explained in literature review. Since there is no production test results or core saturation data; any shaly-sand model`s result that tend to be close or similar to Archie`s result will be considered pessimistic. Therefore, the Archie's model will be used a reference base relative to other models.

Comparison of water saturation from Different Methods

Since the entire reservoir is observed to be a mixture of clean sand at the mid interval and shaly at the top and bottom (**Figure 8**). The average water saturation in clean sand interval was first calculated using all mentioned saturation models applying the same model parameters (**m**, **n**, and **a**).

The purpose is to examine the application of shaly-sand interpretation models in the clean reservoir relative to basic Archie model.

Table 1 through **4)** represents the summary of the important computed petrophysical parameters for the well. All models have shown no significant differences in the average water saturation and other important reservoir properties. **Table 9** shows the summary of all computed parameters with the hydrocarbon saturation ranging from 0.977 to 0.988 for the clean zone with an average porosity of 27.2% from all models. The average permeability for the clean interval is approximately to 6539 mD estimated from the Timur-Coates model.

It is observed that one may attempt to even apply any model (Archie or shaly sand models) in formation with a minimal or null shale contents. However, in a low shaliness reservoir the Archie model still remains the best technique due to few parameters that needs to be computed before applying the model. The shaly sand saturation models involve a clean term (Archie term) and a shale term, then it is now clear that, the shale term drops to zero or insignificant value when the amount of shale vanishes and all shaly saturation equations revert to clean model (Archie model).

Table 1: summary of computed petrophysical parameters (clean sand) for well 7220/8-1 using Archie model

Zones	Flag name	Top (m)	Bottom (m)	Gross (m)	Net (m)	Net to Gross (frac)	BVW	HCPOR-TH	Average Shale Volume (%)	Average porosity (%)	Average water Saturation (%)
Clean sand	ROCK	1335.0	1353.3	18.3	18.3	1	0.37	4.9	0.2	27.2	2.3
Clean sand	RES	1335.0	1353.3	18.3	18.3	1	0.37	4.9	0.2	27.2	2.3
Clean sand	PAY	1335.0	1353.3	18.3	18.3	1	0.37	4.9	0.2	27.2	2.3

Table 2: summary of computed petrophysical parameters (clean sand) for well 7220/8-1 using Indonesian model

Zones	Flag Name	Top (m)	Bottom (m)	Gross (m)	Net (m)	Net to Gross ,fr	BVW	HCPOR-TH	Average shale Volume (%)	Average porosity (%)	Average water Saturation (%)
Clean sand	ROCK	1335.0	1353.3	18.3	18.3	1	0.38	4.9	0.2	27.2	2.3
Clean sand	RES	1335.0	1353.3	18.3	18.3	1	0.38	4.9	0.2	27.2	2.3
Clean sand	PAY	1335.0	1353.3	18.3	18.3	1	0.38	4.9	0.2	27.2	2.3

Table3: summary of computed petrophysical parameters (clean sand) using Simandoux model

Zones	Flag Name	Top (m)	Bottom (m)	Gross (m)	Net (m)	Net to Gross (fr)	BVW	HCPOR-TH	Average Shale Volume (%)	Average Porosity (%)	Average Water Saturation (%)
Clean Sand	**ROCK**	1335.0	1353.3	18.3	18.3	1	0.37	4.9	0.2	27.2	2.2
Clean Sand	**RES**	1335.0	1353.3	18.3	18.3	1	0.37	4.9	0.2	27.2	2.2
Clean Sand	**PAY**	1335.0	1353.3	18.3	18.3	1	0.37	4.9	0.2	27.2	2.2

Table4: summary of computed petrophysical parameters (clean sand) for well 7220/8-1 using Modified Simandoux model

Zones	Flag Name	Top (m)	Bottom (m)	Gross (m)	Net (m)	Net to Gross (fr)	BVW	HCPOR-TH	Average shale Volume (%)	Average Porosity (%)	Average Water Saturation (%)
Clean Sand	ROCK	1335.0	1353.3	18.3	18.3	1	0.37	4.9	0.2	27.2	2.2
Clean Sand	RES	1335.0	1353.3	18.3	18.3	1	0.37	4.9	0.2	27.2	2.2
Clean Sand	PAY	1335.0	1353.3	18.3	18.3	1	0.37	4.9	0.2	27.2	2.2

The even greatest interest of the study is to compare the average water saturation values from all modes considering the entire hydrocarbon interval using Archie as the reference base.

Table 5 through **8)** show the summary of the computed petrophysical parameters considering the entire hydrocarbon-bearing interval. All models have shown different results.

Table 5 summarizes results from Archie model. The model estimated higher water saturation (S_w) relatively to shaly sand models. The reason is being the shale or clays effects. Shale or clays have an important impact on most logging tools such as porosity and resistivity logs. Since S_w is a function of formation resistivity (R_t), porosity (Ø), and water formation resistivity (R_w). The presence of shale or clays lowers (suppress) the formation resistivity by the excess conductivity of shale and clay minerals. Archie assumed that only fluid in the pores is conductive which is opposite to shale matrix being conductive.

Suppression of formation resistivity by the shale effects causes an error that is directly translated to S_w value. This is the source of an overestimation of S_w value from the model.

The apparent differences in the estimated average water saturation values from all shaly sand equations can be expected to vary when the amount of shale or clay in potential zone varies. Not only by varying the amount of shale but also the way the shale is distributed in the potential reservoir.

Table 6 shows summary results from the Indonesian model. The average S_w is relatively higher compared to other two shaly models and is close to that of the Archie model. The Indonesian model demands a relatively higher shale contents reservoir and fresh water reservoir for its effectiveness. Quantitative interpretation has shown that the well penetrated low shale content reservoir this makes the Indonesian model less useful for the study. Since its S_{wavg} value is close to that of Archie`s value the model is considered to overestimate the water saturation.

Table 7 represents summary results from the Simandoux model. The model yields lower results (S_{wavg}) but again is close to that of Archie and Indonesian models. The application of these models demands a type of dispersed shale, low shaliness, and more saline reservoir (low R_w) as found in the literature review. This model demands dispersed shale resistivity which varies with saturation and is more difficult to determine.

Table 8 shows summary of computed petrophysical parameters from the Modified Simandoux model. This model yields the lowest average water saturation (S_{wavg}) than the other two shaly sand models. The application of the model is similar to that of Simandoux with a minor modification made to original Simandoux. A factor of ($1-V_{sh}$) is multiplied to the aR_w term. It is not expected to hold true for other reservoir displaying similar conditions. Because S_w is the function of many parameters that are likely to affect it.

It is again important to remember that uncertainties in the model parameters do exist (**a**, **m**, and **n**). Some parameters may fit in one model and become unrealistically pessimistic to other models. For example, an Indonesian model

may demand an 'a' less than unity and the 'n' values may be varied and produce a considerable differences saturation values.

Table 5: summary of computed petrophysical parameters (Entire zone) for well 7220/8-1 using Archie model

Zones	Flag Name	Top (m)	Bottom (m)	Gross (m)	Net (m)	Net to Gross (fr)	BVW	HCPOR-TH	Average shale Volume (%)	Average porosity (%)	Average water Saturation (%)
Entire	ROCK	1276	1412	136.6	101.3	74.3	19.4	16.8	15.9	24.9	23.3
Entire	RES	1276	1412	136.6	101.3	73	19.3	17.1	15.9	25.3	23.3
Entire	PAY	1276	1412	136.6	87.8	64.4	10.3	18.8	15.2	25	14.3

Table 6: summary of computed petrophysical parameters (Entire zone) for well 7220/8-1 using Indonesian model

Zones	Flag Name	Top (m)	Bottom (m)	Gross (m)	Net (m)	Net to Gross (%)	BVW	HCPOR-TH	Average shale Volume (%)	Average porosity (%)	Average water Saturation (%)
Entire	ROCK	1276	1412	136.6	101.3	74.3	17.5	19.9	15.9	24.9	21.1
Entire	RES	1276	1412	136.6	99.5	7.3	17.5	19.9	15.9	25.3	21.1
Entire	PAY	1276	1412	136.6	89.3	65.5	10	19.3	15.3	25	13.6

Table 7: summary of computed petrophysical parameters (Entire zone) for well 7220/8-1 using Simandoux model

Zones	Flag Name	Top (m)	Bottom (m)	Gross (m)	Net (m)	Net to Gross (%)	BVW	HCPOR-TH	Average shale Volume (%)	Average porosity (%)	Average water Saturation (%)
Entire	ROCK	1276	1412	136.6	101.3	74.3	16.2	20.3	15.9	24.9	19.5
Entire	RES	1276	1412	136.6	99.5	7.3	16.2	20.2	15.9	25.3	19.6
Entire	PAY	1276	1412	136.6	90.4	66.3	9.5	19.7	15.4	25	12.8

Table 8: summary of computed petrophysical parameters (Entire zone) for well 7220/8-1using Modified Simandoux model

Zones	Flag Name	Top (m)	Bottom (m)	Gross (m)	Net (m)	Net to Gross ,%	BVW	HCPOR-TH	Average shale Volume (%)	Average porosity (%)	Average water Saturation (%)
Entire	ROCK	1276	1412	136.6	107	78.4	16.2	22.3	12.4	25.5	18.1
Entire	RES	1276	1412	136.6	105.2	77.1	16.2	22.2	12.4	25.8	18.1
Entire	PAY	1276	1412	136.6	94.3	69.2	7.8	21.9	11.7	25.7	9.8

Table 9: summary of computed petrophysical parameters from all modes

Model	S_{wavg1} (frac)	s_{havg1} (frac)	S_{wavg2} (frac)	s_{havg2} (frac)	Φ_{avg1} (frac)	Φ_{avg2} (frac)	V_{shavg1} (frac)	V_{shavg2} (frac)	S_w/S_{xo} (frac)
Archie	0.023	0.977	0.143	0.857	0.272	0.25	0.002	0.152	0.333
Indonesian	0.023	0.977	0.136	0.864	0.272	0.25	0.002	0.153	0.264
Simandoux	0.022	0.988	0.128	0.872	0.272	0.25	0.002	0.154	0.243
Modified Simandoux	0.022	0.988	0.098	0.902	0.272	0.257	0.002	0.117	0.241

1: represents clean sand zone

2: represents Entire hydrocarbon-bearing zone (shaly sand)

Hydrocarbon Moveability Index (S_w/S_{xo})

This is the fraction of the uninvaded water saturation (S_w) and the flushed zone water saturation (S_{xo})**.** The ratio of the S_w/S_{xo} has an important indication on the moveability of hydrocarbon. For S_w/S_{xo} greater or equivalent to 1 indicating that the hydrocarbon is immoveable. For values less than 0.7 indicating that the hydrocarbon is moveable. Hydrocarbon moveability index has been calculated from all models and all the values are less than 0.7, which indicates that the hydrocarbon for this pay sand reservoir is moveable.

Table 10 represents the hydrocarbon moveability index and hydrocarbon saturation.

Model	**Pay thickness (m)**	**Average water saturation (%)**	**Average** S_w/S_{xo}	**Hydrocarbon saturation (%)**
Archie	371	14.3	0.333	85.6
Indonesian	359.5	11.5	0.264	88.5
Simandoux	355	10.4	0.243	89.6
Modified Simandoux	357.5	10.2	0.241	89.8

Table 10: Hydrocarbon moveability index from all models.

Permeability of Hydrocarbon Zones (k)

Figure 12 Compare the core-derived permeability and the estimated permeability from the KTIM and SDR using NMR logs (track 7). The results show a satisfactory good agreement between the Timur-Coates model and the measured core permeability than the SDR permeability. This model works well in the hydrocarbon-bearing formation provided that the bound volume fluid part do not contain oil or oil filtrate which may cause the estimated permeability from the Timur-coates to be underestimated.

The presence of gas in the formation causes the mean T_2 values much low. Consequently, the estimated permeability by the SDR model is underestimated in hydrocarbon bearing formation. The Schlumberger-Doll-Research model works perfectly in 100% water saturated formation as explained from various literatures. Since the influence of hydrocarbon on T_{2gm} cannot be corrected, the model does not work perfectly in hydrocarbon zones.

For this study, the SDR model (blue curve) underestimated the formation permeability. The average estimated permeability from the SDR method is 566 mD and that of the Timur-Coates model is 1837 mD. The average core permeability in the same interval is 1571 mD. The relatively small overestimation by the Timur-Coates model may be contributed by the uncertainties in the model parameters or effects of hydrocarbon to the model components or other formation factors like grain size and many related factors.

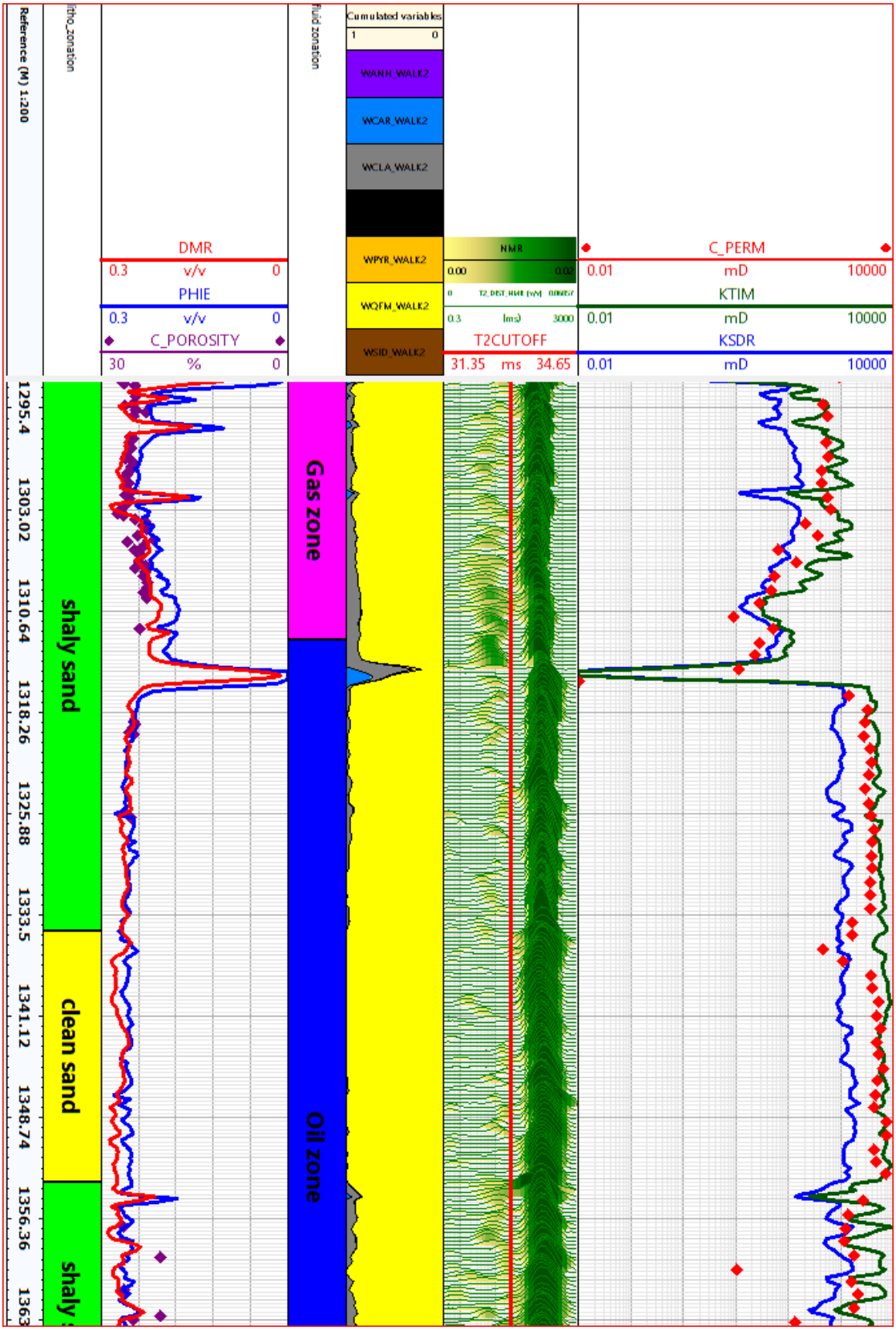

Figure 12: comparison of core-derived permeability (red points) with estimated permeability from Timur-coates (green curve) and SDR (blue curve) using NMR log.

Porosity-Permeability relationship

Permeability is a parameter that tells us how easily the fluid can flow through the porous materials. For well-connected porosity the permeability is expected to vary linearly.

Figure 13 and **Figure 14** show the relationship between effective porosity and the estimated permeability from NMR permeability models. This relationship confirms that the Stø and the Nordmela Formations are permeable with well-connected pores. This linear trend may reflect the deposition sequence within the basin. The presence of shale or clay in the formation may have consequently influenced the formation permeability.

The even good correlation has been shown by the Timur-Coates model with highest regression coefficient value. The trend of these variables may reflect the possible deposition environment which is not part of the study.

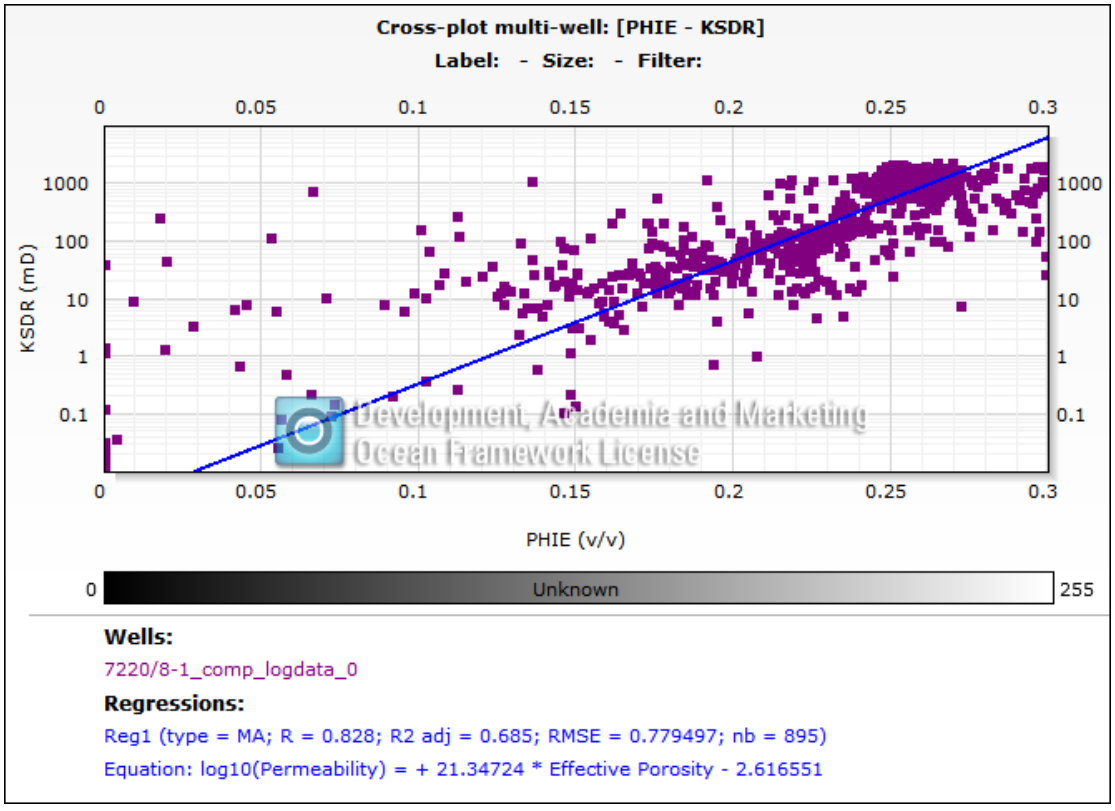

Figure 13: Cross plot Mult-well (PHIE vs KSDR)

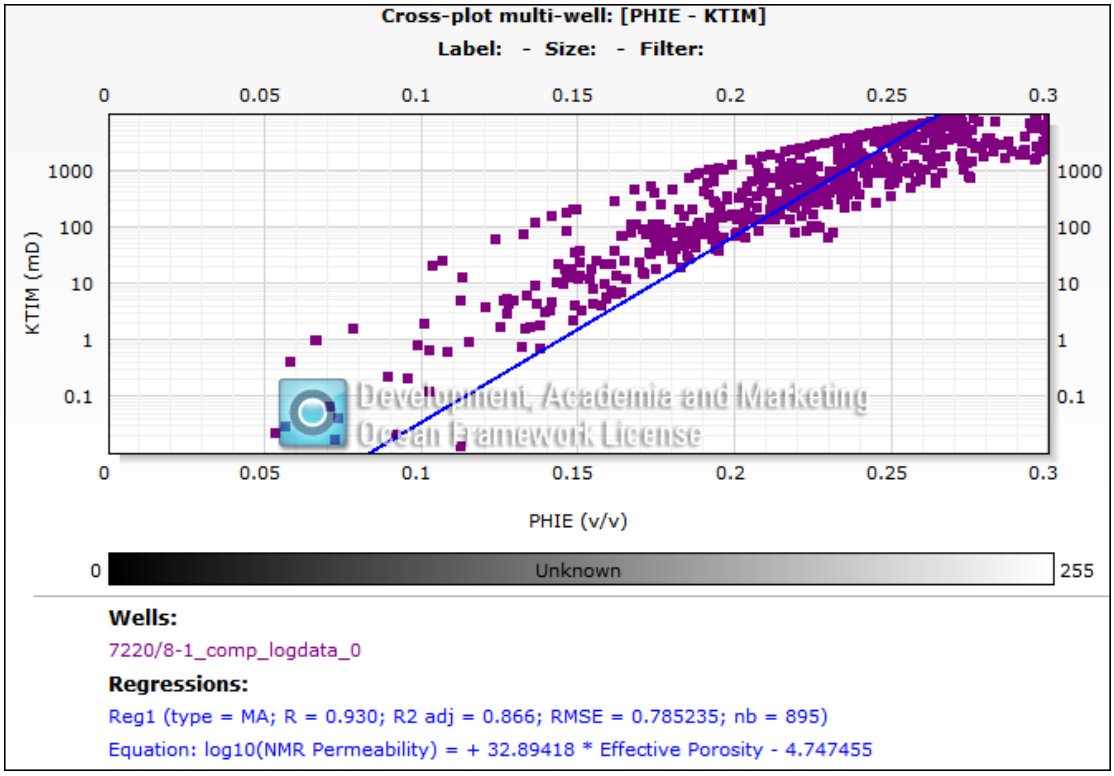

Figure 14: Cross plot Mult-well (PHIE vs KTIM)

7 CONCLUSION AND RECOMMENDATIONS

The interpretation of lithology from both log signatures (characteristics) and Neutron-Density cross plot have confirmed that Stø and Nordmela Formations consists of sands and few amount of shale. Both techniques have also confirmed the presence of carbonate and heavy minerals. These minerals are interpreted to occur in the form of thin cementation (cemented carbonate) such as siderite and heavy minerals (pyrite).

The technique by the Thomas-Stieber for shale distribution has shown that most of shale occurs in the form of laminations with a few percentages dispersed within the pore space of the sands.

The neutron-density porosity interpretation technique underestimated the formation porosity (effective) in the gas interval to a large extent. The combined density delivered porosity and total NMR porosities (DMR) yields good results in the gas-bearing interval when compared to core porosity. Therefore, the DMR method is the most optimistic technique for the study. But also can be applied to other gas-bearing zones.

The technique by the Indonesian model gives higher water saturation values close to that given by Archie model in a potential shaly sand pay interval. Since Archie model overestimates water saturation in shaly sand reservoir and, therefore, the Indonesian technique is regarded to overestimate the water saturation. The method by Simandoux also yields the water saturation close to Indonesian. The even lowest water saturation has been delivered by the Modified Simandoux model. In the clean hydrocarbon-bearing sand interval, all models have proved similar results.

The technique by the SDR model for permeability estimate appears to be unrealistic as compared to core derived permeability in hydrocarbon intervals. The model underestimated the formation permeability to about three times less

to that given by the Timur-Coates. The Timur-Coates model is the most optimistic model (1837 mD average permeability) when compared to core-delivered permeability.

It is recommended that all water saturation interpretation models` results should be checked against water analysis results from core to confirm their accuracy. It is also recommended that model parameters (**a**, **m**, and **n, R_w, and R_{sh}**) should be delivered from laboratory measurements to reduce the uncertainties associated with them.

REFERENCES

Adeoti, L., et al. (2009). An integrated approach to volume of shale analysis: Niger Delta example, Offrire Field. World Applied Sciences Journal **7**(4): 448-452.

Ahmed, U., et al. (1991). Permeability estimation: the various sources and their interrelationships. Journal of petroleum technology **43**(05): 578-587.

Alfosail, K. and A. Alkaabi (1997). Water saturation in shaly formation. Middle East Oil Show and Conference, Society of Petroleum Engineers.

Almon, W. R. (1979). A geologic appreciation of shaly sands. SPWLA 20th Annual Logging Symposium, Society of Petrophysicists and Well-Log Analysts.

Anyaehie, J. C. and O. Olanrewaju (2010). Hydrocarbon Effect Correction on Porosity Calculation from Density Neutron Logs Using Volume of Shale in Niger Delta. Nigeria Annual International Conference and Exhibition, Society of Petroleum Engineers.

Archie, G. E. (1942). The electrical resistivity log as an aid in determining some reservoir characteristics. Transactions of the AIME **146**(01): 54-62.

Berg, C. R. (1996). Effective-medium resistivity models for calculating water saturation in shaly sands. The Log Analyst **37**(03).

Bhatt, A., et al. (2001). Application of committee machines in reservoir characterisation while drilling: a novel neural network approach in log analysis. Proceedings of the Nordic Symposium on Petrophysics, Trondheim, Norway.

Bhuyan, K. and Q. Passey (1994). Clay estimation from GR and neutron-density porosity logs. SPWLA 35th Annual Logging Symposium, Society of Petrophysicists and Well-Log Analysts.

Coates, G. R. and J. L. Dumanoir (1973). A new approach to improved log-derived permeability. SPWLA 14th Annual Logging Symposium, Society of Petrophysicists and Well-Log Analysts.

Dalland, A., Wosrsley, D, & Ofstad, K. (1988). Astratigraphic scheme for the Mesozoic and Cenozoic succession offshore Norway north 62 N. NPD Bull, 4,67.

Darling, T. (2005). Well logging and formation evaluation, Elsevier.

David, S. O., et al. (2015). A Universal Equation to Calculate Shale Volume for Shaly-Sands and Carbonate Reservoirs. SPE Latin American and Caribbean Petroleum Engineering Conference, Society of Petroleum Engineers.

De Waal, J. (1989). Influence of clay distribution on shaly sand conductivity. SPE Formation Evaluation **4**(03): 377-383.

Doré, A. (1995). Barents Sea geology, petroleum resources and commercial potential. Arctic: 207-221.

Doveton, J. (2001). All models are wrong, but some models are useful:"solving" the Simandoux equation. Kansas Geological Survey, University of Kansas, Lawrence, Kansas USA.

Ellis, D. V., et al. (2004). Porosity from neutron logs II: interpretation. Petrophysics **45**(01).

Ellis, D. V. and J. M. Singer (2007). Well logging for earth scientists, Springer Science & Business Media.

Ferns, T. W. (2000). Petrophysical properties from small samples using image analysis techniques. TU Delft, Delft University of Technology.

Fertl, W. and G. V. Chilingar (1988). Determination of volume, type, and distribution modes of clay minerals from well logging data. SPE Formation Damage Control Symposium, Society of Petroleum Engineers.

Fertl, W. H. and G. W. Hammack (1971). A comparative look at water saturation computations in shaly pay sands. SPWLA 12th Annual Logging Symposium, Society of Petrophysicists and Well-Log Analysts.

Fleury, M., et al. (2004). Evaluation of water saturation from resistivity in a carbonate field. From laboratory to logs. Proceedings of International Symposium of the Society of Core Analysts, Abu Dhabi, UAE.

Freedman, R., et al. (1998). Combining NMR and density logs for petrophysical analysis in gas-bearing formations. SPWLA 39th Annual Logging Symposium, Society of Petrophysicists and Well-Log Analysts.

Gaymard, R. and A. Poupon (1968). Response of neutron and formation density logs in hydrocarbon bearing formations. The Log Analyst **9**(05).
Gimbe, M. P. S. (2015). Formation Evaluation and Uncertainty Analysis of the Ormen Lange Field, Norwegian Sea offshore Norway.

Hamada, G. and M. N. Al-Awad (2000). Petrophysical evaluation of low resistivity sandstone reservoirs. Journal of Canadian Petroleum Technology **39**(07).

Hermanrud, C., et al. (2014). Petroleum column-height controls in the western Hammerfest Basin, Barents Sea. Petroleum Geoscience **20**(3): 227-240.

Hill, H., et al. (1979). Bound Water In Shaly Sands-Its Relation To Q And Other Formation Properties. The Log Analyst **20**(03).

Ijasan, O., et al. (2013). Estimation of Porosity and Fluid Constituents from Neutron and Density Logs Using an Interactive Matrix Scale. SPWLA 54th Annual Logging Symposium, Society of Petrophysicists and Well-Log Analysts.

Kamel, M. H. and W. M. Mabrouk (2003). Estimation of shale volume using a combination of the three porosity logs. Journal of Petroleum Science and Engineering **40**(3): 145-157.

Kleinberg, R. and H. Vinegar (1996). NMR properties of reservoir fluids. The Log Analyst **37**(06): 20-32.

Kukal, G. C. and R. E. Hill (1986). Log Analysis Of Clay Volume: An Evaluation Of Techniques And Assumptions Used In An Upper Cretaceus Sand-Shale Sequence. SPWLA 27th Annual Logging Symposium, Society of Petrophysicists and Well-Log Analysts.

La Vigne, J., et al. (1994). Density-neutron interpretation in shaly sands. SPWLA 35th Annual Logging Symposium, Society of Petrophysicists and Well-Log Analysts.

Lin, J. L. and H. Salisch (1994). Determination from well logs of porosity and permeability in a heterogeneous reservoir. SPE Asia Pacific Oil and Gas Conference, Society of Petroleum Engineers.

Mackenzie, R. (1959). The classification and nomenclature of clay minerals. Clay Minerals Bull **4**(21): 52-66.

Mao, Z.-Q. (2001). The physical dependence and the correlation characteristics of density and neutron logs. Petrophysics **42**(05).

McCarney, E. R., et al. (2015). Core Plug Nuclear Magnetic Resonance (NMR) Analysis as a Method to Estimate Permeability Anisotropy. SPWLA 56th Annual Logging Symposium, Society of Petrophysicists and Well-Log Analysts.

Ohm, S. E., et al. (2008). Geochemically driven exploration models in uplifted areas: Examples from the Norwegian Barents Sea. AAPG bulletin **92**(9): 1191-1223.

Poupon, A., et al. (1970). Log Analysis of Sand-Shale SequencesA Systematic Approach. Journal of petroleum technology **22**(07): 867-881.

Poupon, A. and R. Gaymard (1970). The evaluation of clay content from logs. SPWLA 11th Annual Logging Symposium, Society of Petrophysicists and Well-Log Analysts.

Poupon, A. and J. Leveaux (1971). Evaluation of water saturation in shaly formations. SPWLA 12th Annual Logging Symposium, Society of Petrophysicists and Well-Log Analysts.

Poupon, A., et al. (1954). A contribution to electrical log interpretation in shaly sands. Journal of petroleum technology **6**(06): 27-34.

Quintero, L. F. and Z. Bassiouni (1998). Porosity determination in gas-bearing formations. SPE Permian Basin Oil and Gas Recovery Conference, Society of Petroleum Engineers.

Riis, F. and W. Fjeldskaar (1992). On the magnitude of the Late Tertiary and Quaternary erosion and its significance for the uplift of Scandinavia and the Barents Sea. Structural and tectonic modelling and its application to petroleum geology, Elsevier Amsterdam. **1:** 163-185.

Ruhovets, N. and W. H. Fertl (1982). Volumes, Types, and Distribution of Clay Minerals in Reservoir Rocks Based on Well Logs. SPE Unconventional Gas Recovery Symposium, Society of Petroleum Engineers.

Soto Becerra, R., et al. (2010). The Correct Shale-Volume Characterization Increases Hydrocarbon Reserves: Case Study of Cretaceous Formation, Lake of

Maracaibo, Venezuela. SPE Latin American and Caribbean Petroleum Engineering Conference, Society of Petroleum Engineers.

Thern, H. F. and S. Chen (1999). A deterministic method for gas reservoir evaluation using dual wait-time NMR and density log data. SPE Annual Technical Conference and Exhibition, Society of Petroleum Engineers.

Thomas, E. and S. Stieber (1975). The distribution of shale in sandstones and its effect upon porosity. SPWLA 16th annual logging symposium, Society of Petrophysicists and Well-Log Analysts.

Tyurin, E., Borghi, M., Gossenberge, P., Pirrone, M., & Cominesi, N. R. (2015). Alternative Approach to Absolute Permeability Using NRM-Derived Grain Size Distribution. Paper presented at the Offshore Mediterranean Conference and Exhibition.

Waxman, M. and L. Smits (1968). Electrical conductivities in oil-bearing shaly sands. Society of Petroleum Engineers Journal **8**(02): 107-122.

Worthington, P. F. (1985). The evolution of shaly-sand concepts in reservoir evaluation. The Log Analyst **26**(01).

Xiao, L., Liu, X.-P., Zou, C.-C., Hu, X.-X., Mao, Z.-Q., Shi, Y.-J., . . . Li, G.-R. (2014). Comparative study of models for predicting permeability from nuclear magnetic resonance (NMR) logs in two Chinese tight sandstone reservoirs. *Acta Geophysica, 62*(1), 116-141.

Web references

Norwegian Directorate factpages: http://factpages.npd.no/factpages/Default.aspx?culture=en&nav1=wellbore&nav2=PageView|Exploration|All&nav3=6484, visited: 25.3.2016.

APPENDIX

APPENDIX A

Cross-plots of compatible logs for well 7220/8-1

A1. Neutron-density cross-plot for **Zone_1** marked in **Figure 8**

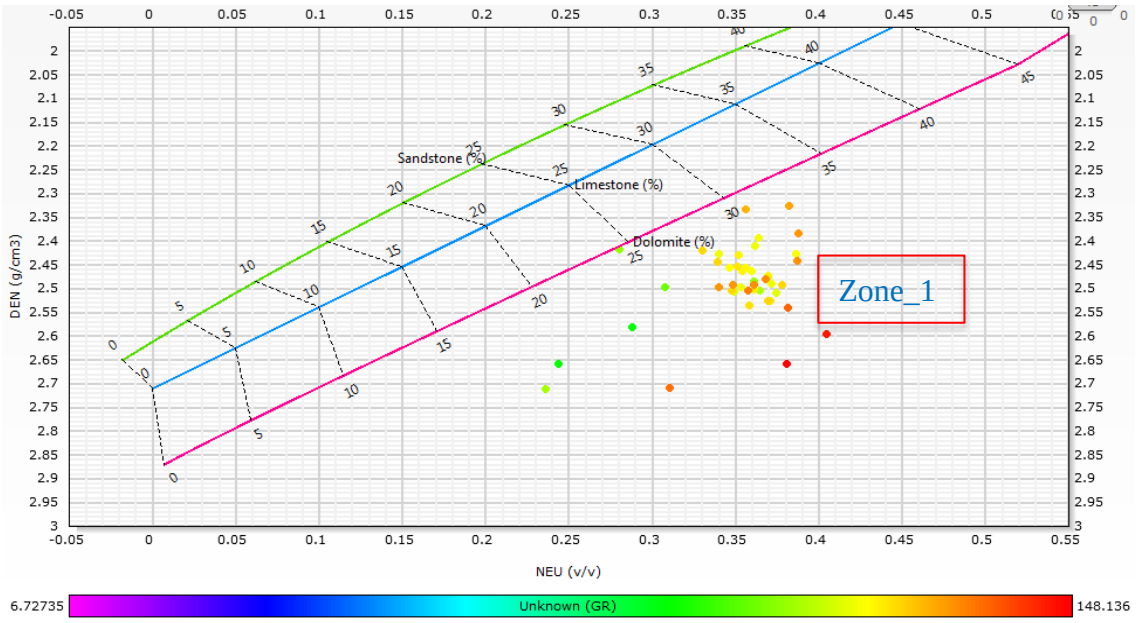

A2. Neutron-density cross-plot for **Zone_2** marked in **Figure 8**

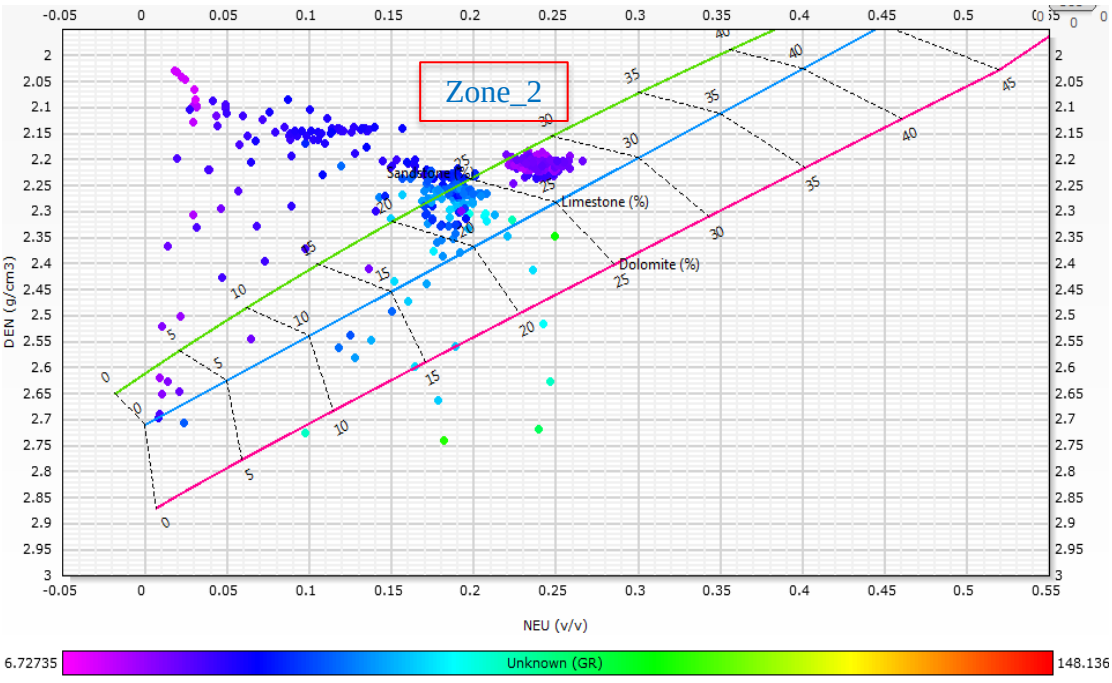

A3. Neutron-density cross-plot for **Zone_4** marked in **Figure 8**

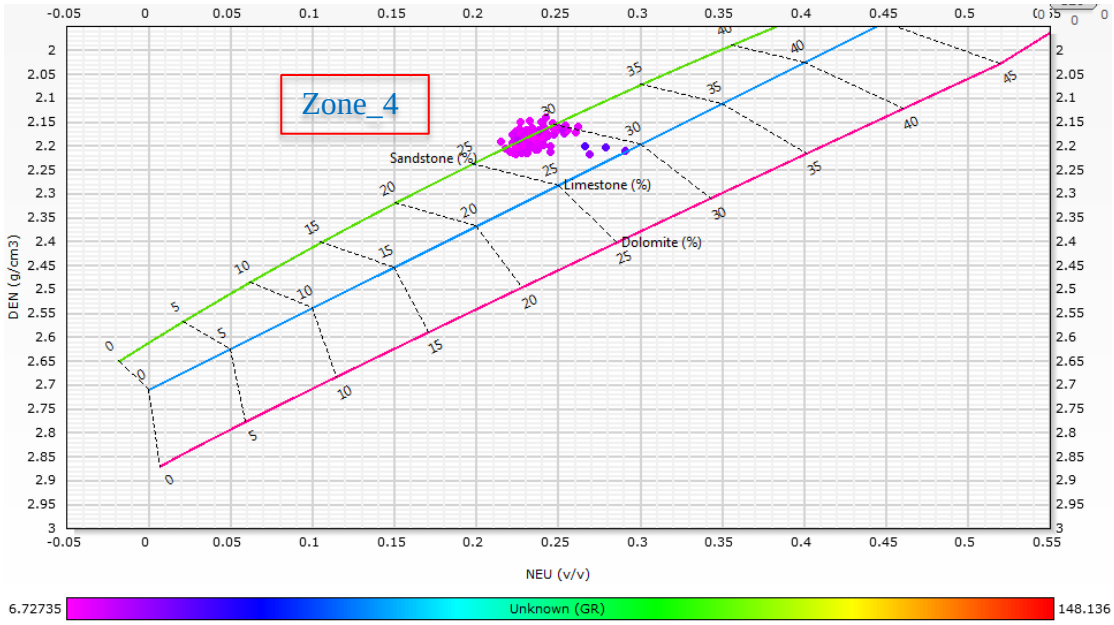

A4. Neutron-density cross-plot for **Zone_5, 6, and 7** marked in **Figure 8**

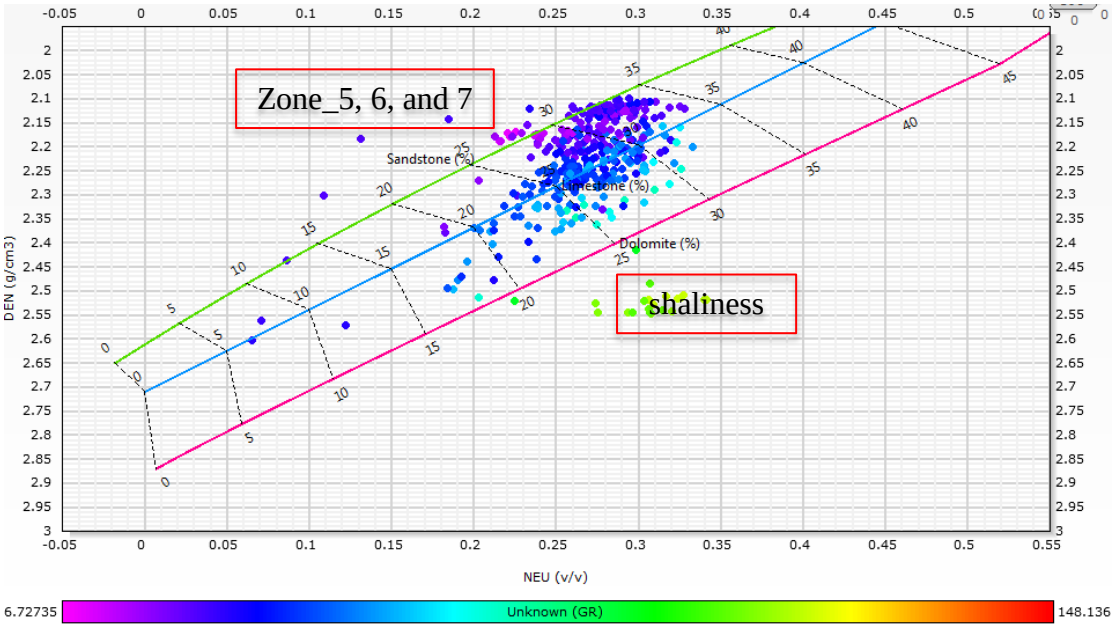

Appendix B

Petrophysical calculation curves from the well 7220/8-1

B1. Petrophysical shale volume ($\mathbf{V_{sh}}$) calculation curves for linear GR, nonlinear GR, and neutron-density Models

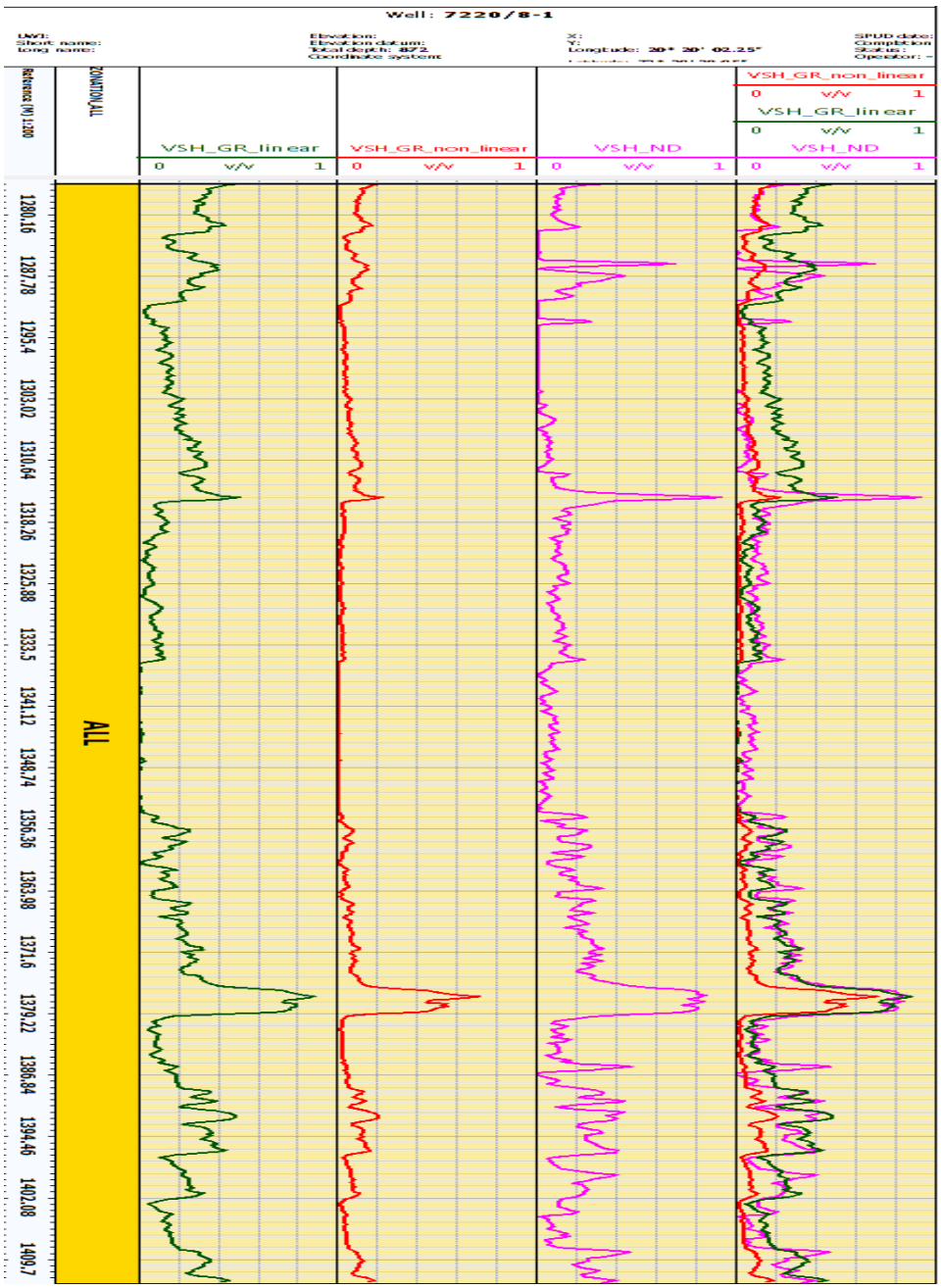

B2. Petrophysical porosity (Ø) calculation curves for a neutron-density and density-magnetic resonance Models

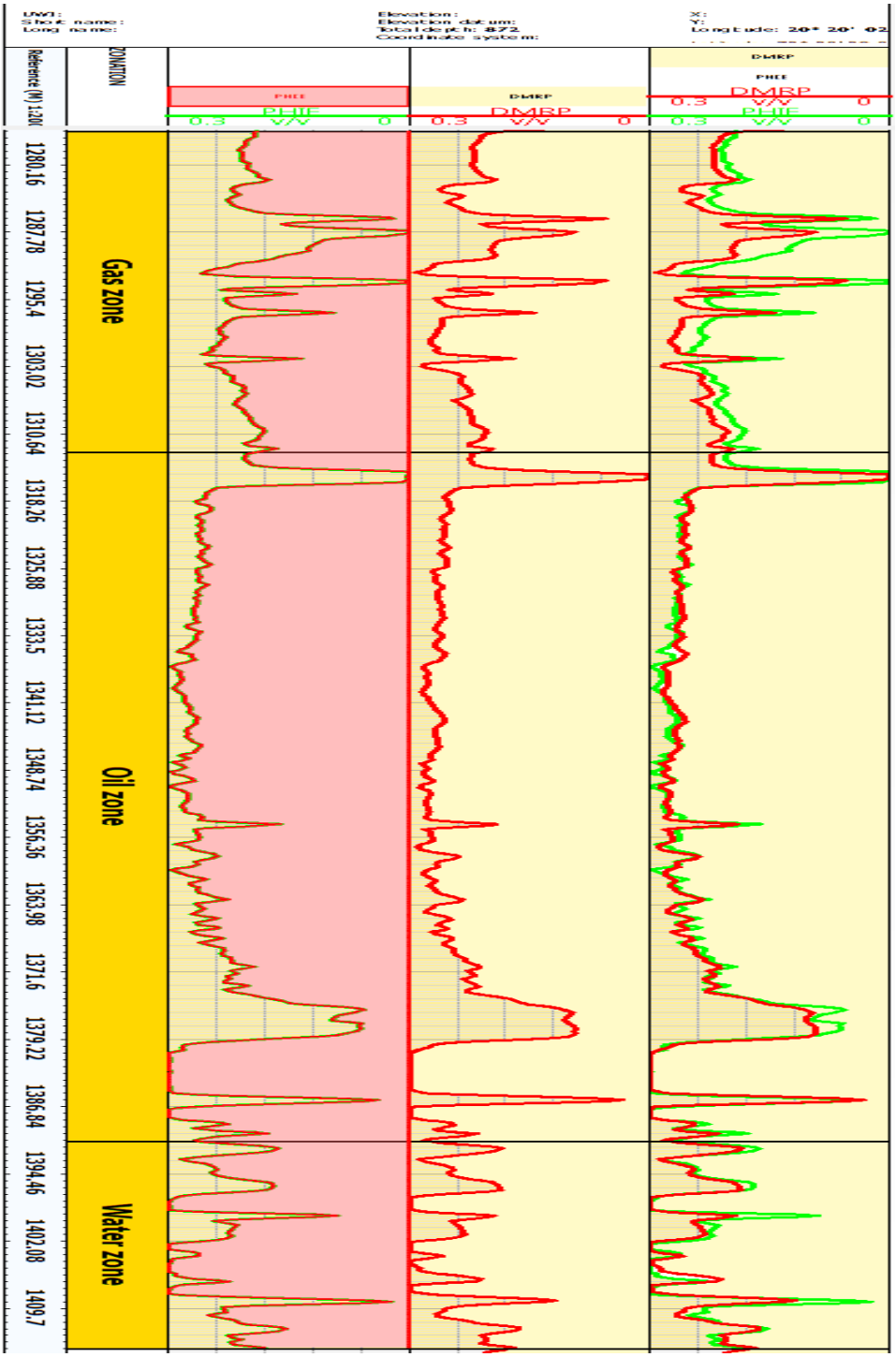

B3. Petrophysical water saturation **(S_w)** calculation curves for all saturation models

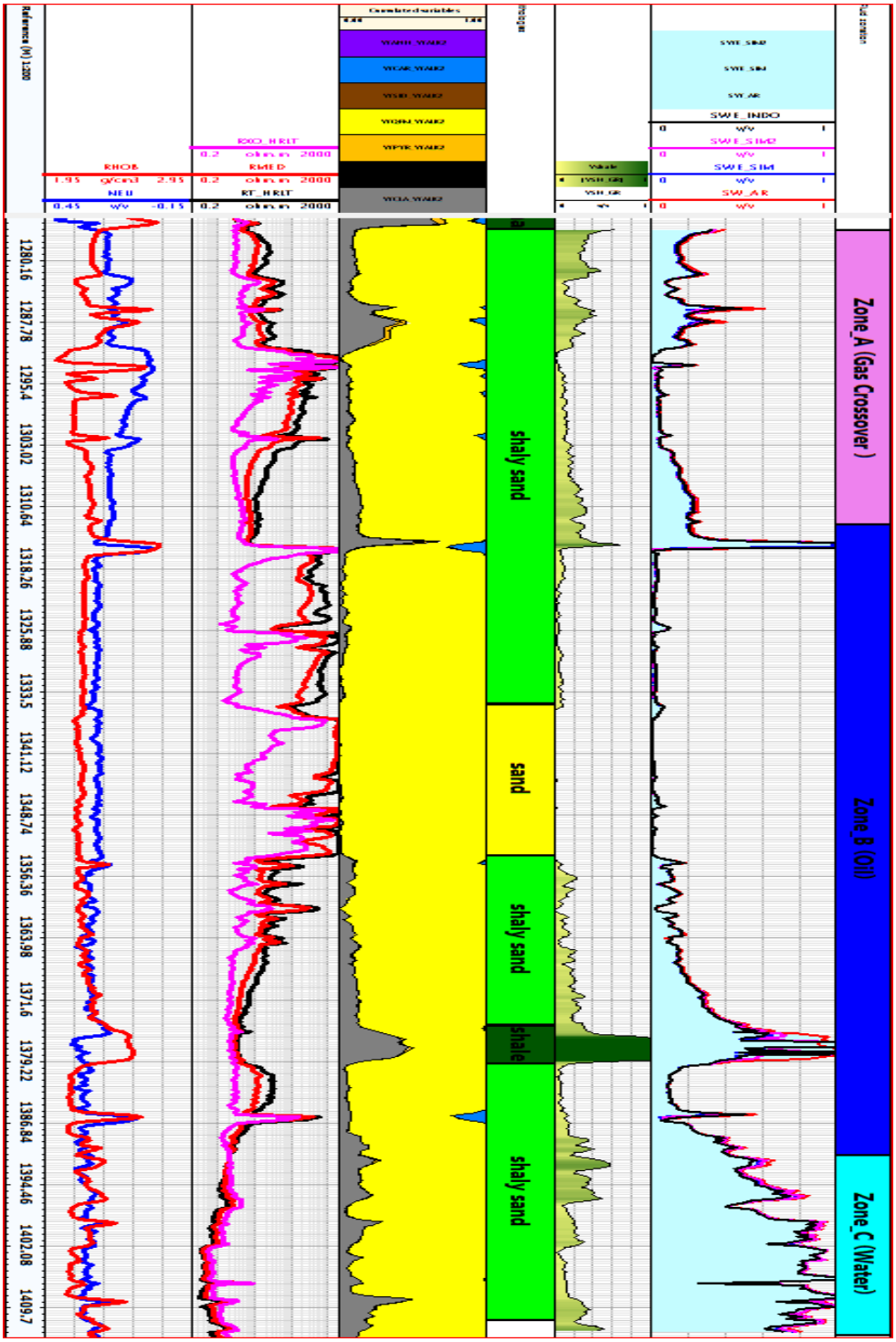

Appendix C

Thomas-Stieber cross-plots for shale distribution

C1. Shale distribution from Gamma ray-porosity cross plot for **Zone_2** as shown in **Figure 8**

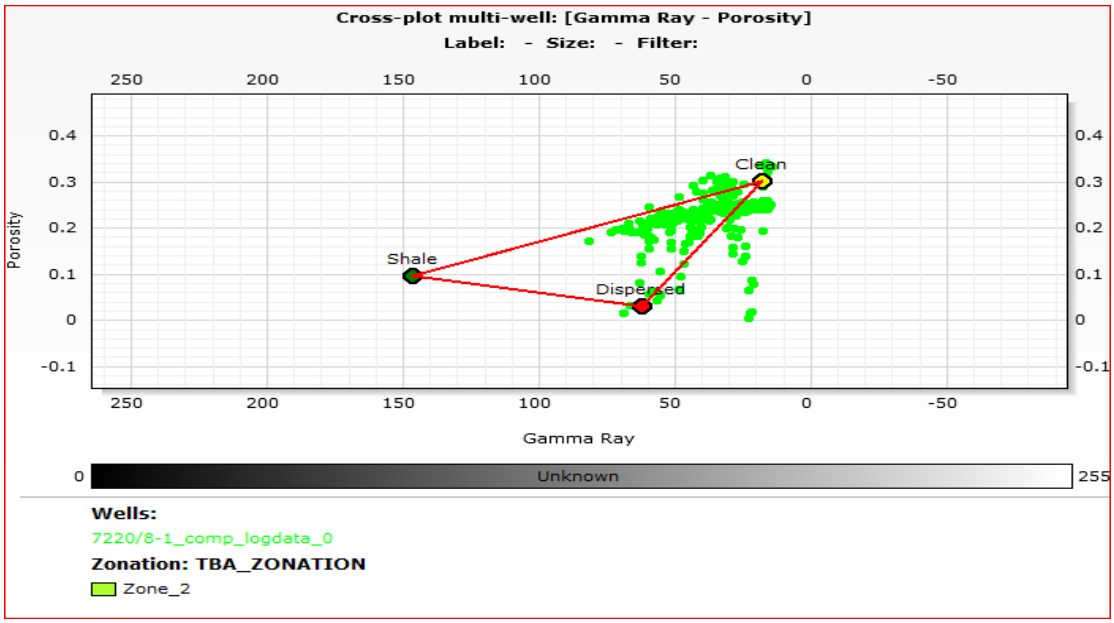

C2. Shale distribution from Gamma ray-porosity cross plot for **Zone_4** as shown in **Figure 8**

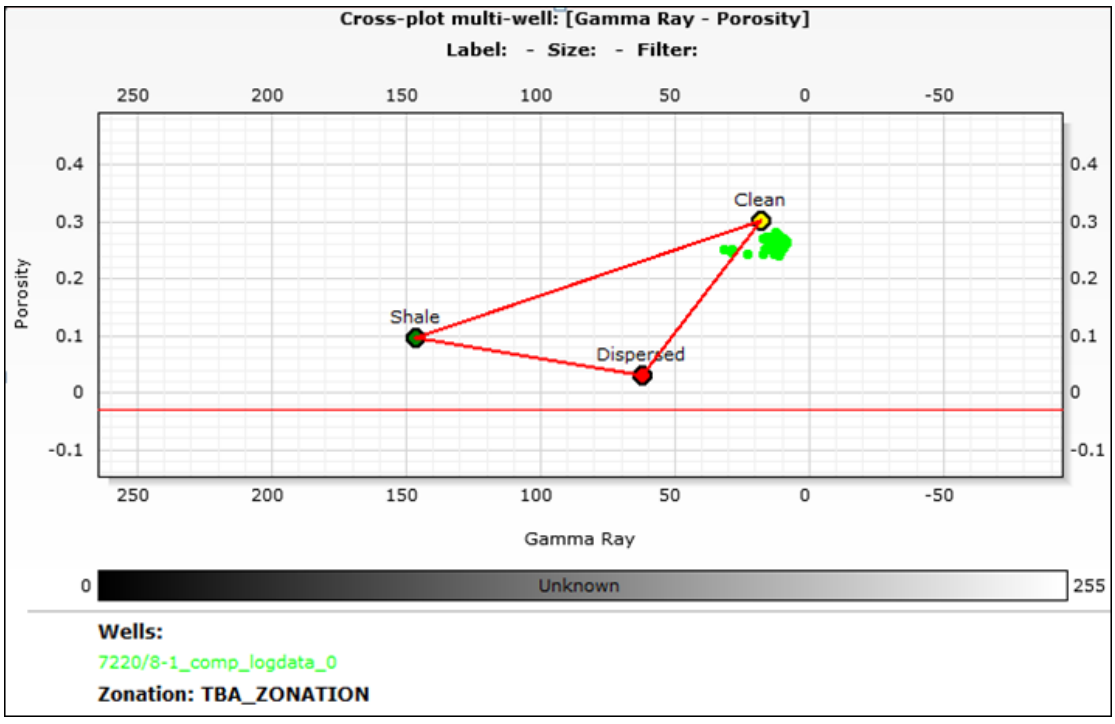

C3. Shale distribution from Gamma ray-porosity cross plot for **Zone_5** as shown in **Figure 8**

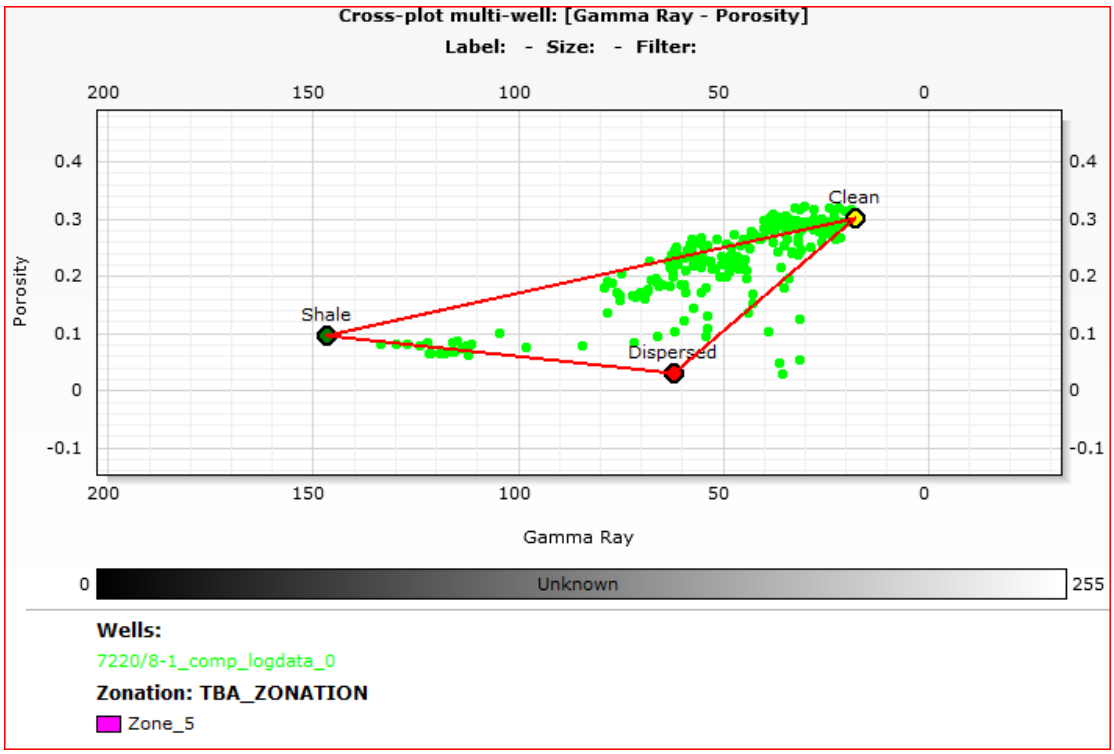

C4. Shale distribution from Gamma ray-porosity cross plot for **Zone_7** as shown in **Figure 8**

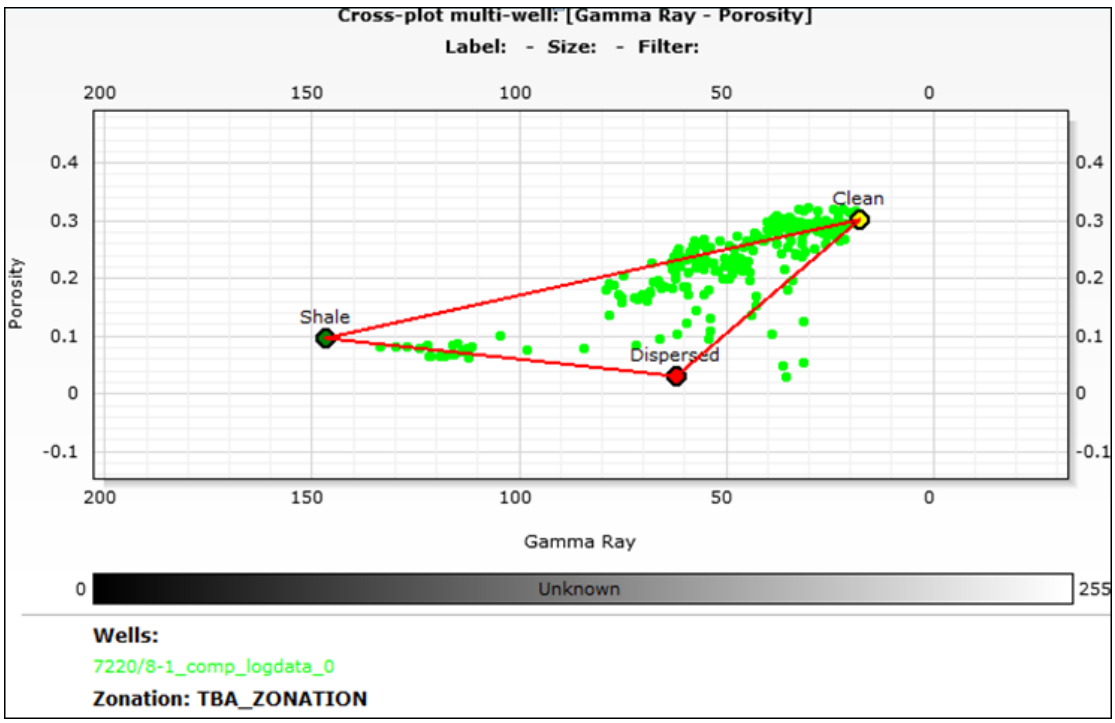

C5. Shale distribution from Gamma ray-porosity cross plot for all hydrocarbon zones (**Zone_2 to Zone_7**) as marked in **Figure 8**